HHS Public Access

Author manuscript

Cell Rep. Author manuscript; available in PMC 2024 June 23.

Published in final edited form as:

Cell Rep. 2024 May 28; 43(5): 114202. doi:10.1016/j.celrep.2024.114202.

The Janus kinase 1 is critical for pancreatic cancer initiation and progression

Hridaya Shrestha[1], **Patrick D. Rädler**[1,2,9], **Rayane Dennaoui**[1], **Madison N. Wicker**[1], **Nirakar Rajbhandari**[2,10], **Yunguang Sun**[3], **Amy R. Peck**[4], **Kerry Vistisen**[1], **Aleata A. Triplett**[2], **Rafic Beydoun**[1,5], **Esta Sterneck**[6], **Dieter Saur**[7,8], **Hallgeir Rui**[4], **Kay-Uwe Wagner**[1,11,*]

[1]Department of Oncology, Wayne State University School of Medicine and Tumor Biology Program, Barbara Ann Karmanos Cancer Institute, Detroit, MI 48201, USA

[2]Eppley Institute for Research in Cancer and Allied Diseases, University of Nebraska Medical Center, Omaha, NE 68198, USA

[3]Department of Pathology, Medical College of Wisconsin, Milwaukee, WI 53226, USA

[4]Department of Pharmacology, Physiology & Cancer Biology, Thomas Jefferson University, Philadelphia, PA 19107, USA

[5]Department of Oncology, Wayne State University School of Medicine, Detroit, MI 48201, USA

[6]Laboratory of Cell and Developmental Signaling, Center for Cancer Research, National Cancer Institute, Frederick, MD 21702, USA

[7]Division of Translational Cancer Research, German Cancer Research Center (DKFZ) and German Cancer Consortium (DKTK), Heidelberg, Germany

[8]Translational Cancer Research and Institute of Experimental Cancer Therapy, Klinikum rechts der Isar, Technische Universität München, Munich, Germany

[9]Present address: University of North Carolina, 125 Mason Farm Rd., Chapel Hill, NC 27514, USA

*Correspondence: kuwagner@wayne.edu.

AUTHOR CONTRIBUTIONS

K.-U.W. formulated the overarching research goals and aims, supervised the research, and wrote the manuscript. H.S. performed most of the *in vivo* and cell culture experiments, immunoblots, and immunofluorescent staining techniques. P.D.R. conducted computational analyses of RNA sequencing and nCounter datasets and performed immunofluorescence staining experiments. R.D. assisted with the analyses of human PDAC cell lines, collection of tissue specimens, immunostaining, and retroviral vector production. M.N.W. maintained cell lines, collected tissues, and conducted xenografting experiments. N.R. assisted in the generation and initial analysis of the genetically engineered PDAC mouse models and derived cancer cell lines. R.B. provided expertise in histopathology. K.V. and A.A.T. helped draft institutional animal study protocols, maintained the animal colony, executed the processing of tissues, and developed PCR genotyping protocols. E.S. provided expertise and reagents to study CEBPD gene function. D.S. developed the genetic mouse strains for the pancreas-specific gene deletion and assisted in the application of these strains for this project. H.R. provided normal and malignant human pancreatic tissues and worked with Y.S. and A.R.P. to conduct the associated immunostaining experiments and quantitative imaging analyses.

DECLARATION OF INTERESTS

The authors declare no competing interests.

SUPPLEMENTAL INFORMATION

Supplemental information can be found online at https://doi.org/10.1016/j.celrep.2024.114202.

[10]Present address: Department of Surgery, Division of Surgical Oncology, Moores Cancer Center, University of California San Diego, La Jolla, CA 92093, USA

[11]Lead contact

SUMMARY

Interleukin-6 (IL-6)-class inflammatory cytokines signal through the Janus tyrosine kinase (JAK)/signal transducer and activator of transcription (STAT) pathway and promote the development of pancreatic ductal adenocarcinoma (PDAC); however, the functions of specific intracellular signaling mediators in this process are less well defined. Using a ligand-controlled and pancreas-specific knockout in adult mice, we demonstrate in this study that JAK1 deficiency prevents the formation of $KRAS^{G12D}$-induced pancreatic tumors, and we establish that JAK1 is essential for the constitutive activation of STAT3, whose activation is a prominent characteristic of PDAC. We identify CCAAT/enhancer binding protein δ (C/EBPδ) as a biologically relevant downstream target of JAK1 signaling, which is upregulated in human PDAC. Reinstating the expression of C/EBPδ was sufficient to restore the growth of JAK1-deficient cancer cells as tumorspheres and in xenografted mice. Collectively, the findings of this study suggest that JAK1 executes important functions of inflammatory cytokines through C/EBPδ and may serve as a molecular target for PDAC prevention and treatment.

In brief

Shrestha et al. demonstrate that JAK1 is a key signaling mediator of cytokines that promote mutant KRAS-induced pancreatic cancer initiation and progression. They provide experimental evidence that deficiency in JAK1 prevents tumor formation, and they identified C/EBPδ as a critical downstream effector of the pro-tumorigenic functions of JAK1/STAT signaling.

Graphical abstract

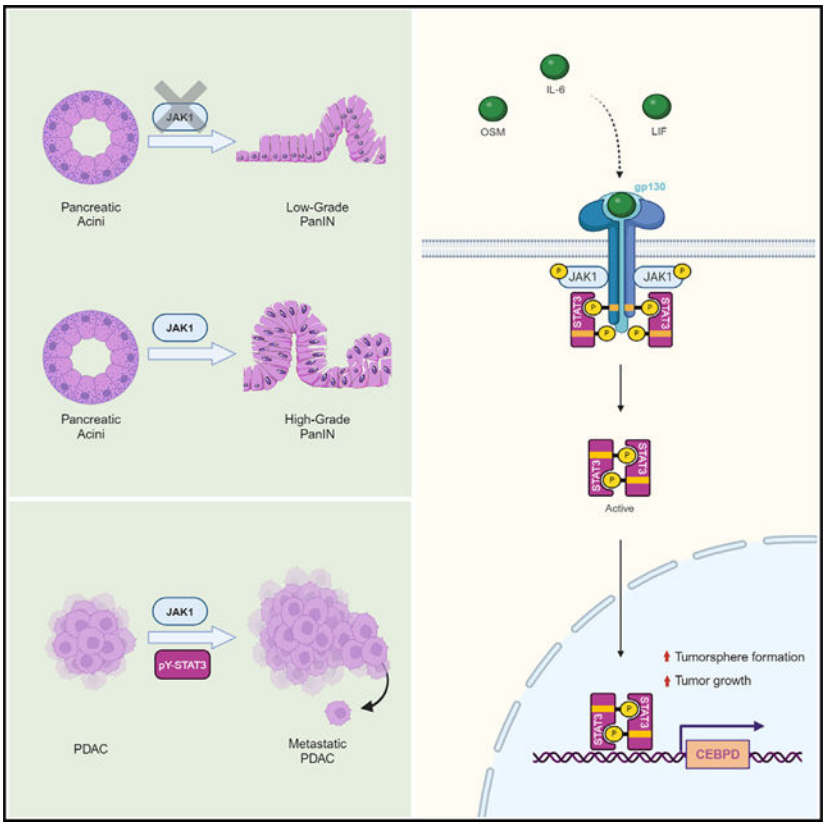

INTRODUCTION

Most pancreatic ductal adenocarcinomas (PDACs) are driven by gain-of-function mutations in *KRAS* along with genetic and epigenetic alterations in tumor susceptibility loci such as *TP53* and *CDKN2A*.[1,2] Besides the well-established importance of these main oncogenic drivers, epidemiological and experimental evidence shows that environmental factors that cause inflammation play key roles in the etiology of pancreatic cancer (for references see review by Dennaoui et al.[3]). Inflammatory cytokines produced by the cancer cells and the tumor microenvironment are important mediators for cancer initiation and metastatic progression.[4–6]

Interleukin-6 (IL-6)-class cytokines (e.g., IL-6, LIF, OSM) are key regulators of inflammation and rational targets for therapy.[7] In support of this notion, work by Shi et al.[8] demonstrated that the inhibition of the leukemia inhibitory factor (LIF) or deficiency of its receptor significantly blocked the initiation of mutant KRAS-induced PDAC. It was also recently proposed that other interleukins (i.e., IL-4 and IL-13) promote the proliferation of cancer cells through metabolic reprogramming.[9] A commonality of these growth factors is that they engage with specific receptor complexes that rely on Janus tyrosine kinases (JAKs) and associated signal transducer and activator of transcription (STAT) proteins for tumor cell-intrinsic signal transduction. Specifically, IL-6-class cytokine receptors share the glycoprotein 130 (gp130) subunit that activates STAT3 in cancer cells. The tyrosine phosphorylation and nuclear location of STAT3 is a hallmark of many malignancies and

coincides with the formation of pancreatic precursor lesions.[10–12] The conditional deletion of the *Stat3* gene in the exocrine pancreas was sufficient to prevent the development of primary and metastatic tumors.[11,12] However, the paradigm of STAT3 as an oncogene has recently been challenged by D'Amico et al.,[13] who proposed that this transcription factor might be critical for the epithelial identity of pancreatic cancer cells, thereby facilitating tumor-suppressive functions.

The inhibition of STAT3 in adenocarcinomas is the subject of intense investigations, and pharmacological agents that directly target this transcription factor or its upstream kinases are currently being tested in preclinical trials.[14–16] Thus far, the treatment of adenocarcinomas with JAK inhibitors has not been successful, and it has remained uncertain whether the activation of STAT3 in pancreatic cancer is regulated by Janus kinases. Our team generated conditional knockout mouse models that lack JAK2 and JAK1[17,18] to assess the biological significance of individual Janus kinases as well as to identify and validate critical downstream targets. Using these models, we recently showed that JAK1 primarily controls the activation of STAT3 in normal and neoplastic mammary epithelial cells.[19,20] The lines of investigation presented in this work are to establish the degree of functional conservation of JAK/STAT signaling cascades in pancreatic tumor cells and to determine whether JAK1 is a rational target in PDAC to block active STAT proteins. The deletion of JAK1 in mice expressing mutant KRAS and in pancreatic cancer cell lines demonstrated that this tyrosine kinase promotes the onset and progression of pancreatic cancer through the activation of multiple STAT proteins (STAT3, 1, and 6) and their transcriptional targets. Moreover, we identified and validated CCAAT/enhancer binding protein δ (C/EBPδ) as a critical downstream effector, which executes important functions of inflammatory cytokine signaling through JAK1. Targeting the JAK1-C/EBPδ signaling cascade might be a suitable strategy for PDAC prevention and treatment.

RESULTS

Expression of JAK1 and constitutive activation of STAT3 and STAT1 in PDAC

We performed a comprehensive analysis of the expression of JAK1 and JAK2 and the activation of five downstream STAT proteins (STAT1, 3, 5a/b, and STAT6) in nine commonly used human pancreatic cancer cell lines and untransformed pancreatic cells (HPNE) (Figures 1A and S1A). The immunoblot analysis showed that both JAKs are expressed at various levels in pancreatic cancer cell lines and untransformed HPNE cells. Relative to the expression in HPNE cells, the levels of JAK1 were elevated in three of the cancer cell lines and lower in Hs766T cells. Despite variations among three experimental repeats, the expression of JAK2 was noticeably lower in six cancer cell lines (Figure S1A). Under normal growth conditions, five out of nine cancer cell lines exhibited significantly higher steady-state levels of tyrosine phosphorylated STAT3, and only two cancer cell lines (Capan-2 and Hs766T) showed a prominently elevated activation of STAT1. Interestingly, five cancer cell lines exhibited a significant reduction in STAT1 activation compared to untransformed cells (Figure S1A) and none of the pancreatic cell lines expressed tyrosine phosphorylated STAT5 and STAT6 in steady state without the administration of exogenous ligands such as growth hormone (hGH) or IL-4 (Figure 1A).

To assess the activation of STAT3 in patient-derived specimens, we conducted a quantitative immunofluorescent analysis of tyrosine phosphorylated STAT3 (pSTAT3) on 28 PDAC cases and 17 normal pancreata (Figure 1B). Given the expression of active STAT3 in the tumor-associated stroma, the tissues were co-stained for pan-cytokeratin to discriminate the nuclear localization of pSTAT3 in cancer cells. While pSTAT3 was detected in a few areas of normal pancreata, the number of cases expressing active STAT3 was significantly higher in pancreatic cancer cells (Figure 1B). Moreover, tumor-derived inflammatory cytokines can impose a field effect that leads to a significantly elevated activation of STAT3 in untransformed exocrine cells as determined by the analysis of pSTAT3 expression on a second set of tissue specimens consisting of 29 cancer cases along with 20 normal pancreatic tissues adjacent to the tumor (NAT) and five normal control pancreata (Figure S1B). The collective observations on primary tumor specimens and human cancer cell lines show that the constitutive activation of the JAK/STAT3 pathway is a common feature in pancreatic cancer. Notably, high activation of STAT3 did not closely match the expression of JAK2 (e.g., Capan-2, Panc-1 cells). JAK1 is abundantly expressed in most pancreatic cancer cell lines, suggesting that JAK1 might be the pivotal tyrosine kinase for the activation of STAT3.

JAK1 deficiency prevents the formation of mutant KRAS-induced high-grade preneoplasia and pancreatic tumors

To determine the significance of JAK1 signaling in pancreatic cancer, we initially used a conventional approach to conditionally delete both copies of the *Jak1* gene in the pancreata of mice that express the $KRAS^{G12D}$ oncogene in a Cre-dependent manner and under a tetracycline-controlled transactivator (Pdx1-Cre CAG-LSL-tTA TetO-$Kras^{G12D}$ $Jak1^{fl/fl}$).[21] In this model, we did not find any $KRAS^{G12D}$-induced precursor lesions in 3- and 6-month-old animals (Figure S2A). This finding might suggest that JAK1 is required for the development of pancreatic preneoplasia, but the outcome of this experiment was inconclusive. The absence of premalignant lesions was possibly the consequence of a negative selection of Pdx1-Cre-expressing exocrine cells that lack JAK1 and expression of mutant KRAS. Using a Cre/lox reporter transgene (CAG-LSL-GFP) to track individual cells with a JAK1 deletion, we found that, in comparison to littermate controls expressing JAK1, pancreata of Pdx1-Cre $Jak1^{fl/fl}$ CAG-LSL-GFP mice exhibited a significant reduction in GFP fluorescence, which is indicative of a selection against JAK1 knockout cells during early development (Figure S2B). To circumvent a negative selection of knockout cells, we established a more advanced genetic model where JAK1 is conditionally deleted in the pancreata of adolescent or adult mice. The model relies on the tamoxifen (Tam)-inducible Cre recombinase (Cre^{ERT2}), whose expression is activated in the pancreas with a *Pdx1* promoter-driven transgene expressing the Flp recombinase (Figure S3A). Simultaneously, Flp activates the expression of mutant KRAS from its engineered endogenous locus (*FSF-*$Kras^{G12D}$) to initiate the formation of pancreatic neoplasms. The deletion of JAK1 was accomplished by treating animals with Tam, which also activated the expression of the CAG-LSL-GFP reporter transgene that was used to monitor the functionality of the Cre^{ERT2} on the single-cell level. Strong activation of GFP and the ligand-controlled deletion of JAK1 were observed in the pancreata of adult Tam-treated experimental animals that carried the Pdx1-Flp, $Rosa26^{CAG\text{-}FSF\text{-}CreERT}$, and CAG-LSL-GFP transgenes in the presence of *Jak1*

conditional knockout alleles (Figures 2A and 2B). The permanent expression of GFP, even months after Tam administration, is evidence that JAK1 is not needed for the survival of exocrine cells in the fully developed pancreas. On the histological level, the Tam-treated knockout glands were indistinguishable from untreated experimental mice (Figure S3B). Despite strong and widespread GFP fluorescence throughout the pancreas, we observed small areas that did not express the reporter, indicative of a minimal mosaic expression of one or more transgenes (Figure 2C, asterisk).

While JAK/STAT signaling is largely inactive during normal tissue homeostasis, the expression of oncogenic *KRAS*^{G12D} in a Flp recombinase-inducible manner (Pdx1-Flp *FSF-Kras*^{G12D}) led to an activation of STAT3 and STAT1 (Figure 2D). The Tam-mediated deletion of JAK1 resulted in a concurrent decline in tyrosine phosphorylated STAT3 and STAT1, suggesting that the persistent oncogenic activation of these STATs is mediated by JAK1. The expression of mutant KRAS in control mice caused a widespread development of precursor lesions, most of which were high-grade pancreatic intraepithelial neoplasia (PanIN). In contrast, Tam-treated experimental mice presented low-grade PanINs that were composed of columnar to cuboidal cells with varying amounts of mucins and very mild degrees of cytological and architectural atypia (Figure 2E). The tall columnar and cuboidal epithelial cells in the low-grade lesions did not express any nuclear STAT3 (Figure 2F, middle). The observed differences in the precursor subtype might be primarily due to the lack of JAK1 since Tam-treated mice with only one conditional *Jak1* knockout allele exhibited GFP-positive high-grade PanINs with few areas of low-grade preneoplastic lesions (Figure 2F, right). Low-magnification images illustrate the widespread differences in the histopathology between the JAK1 conditional knockouts and wild-type controls (Figure S4A). More importantly, the high-grade PanINs in the pancreata of JAK1-expressing mice had significantly more Ki67-positive proliferating cells compared to the low-grade precursor lesions in the JAK1 knockouts (Figure S4B).

Among five experimental mice treated early with Tam (i.e., before or shortly after weaning), only one mouse developed a palpable pancreatic tumor after more than 12 months. This tumor and the adjacent acinar cells exhibited a variable expression of GFP, and nuclear STAT3 was present in GFP-negative cells (Figure 2G, left). The GFP-negative tumor cells likely originated from cells that did not undergo Cre^{ERT2}-mediated recombination, such as those shown in Figure 2C. We also investigated the potential effects of deleting JAK1 in the pancreata of experimental mice with established precursor lesions. Among 11 mice treated with Tam around 6 months of age, only one animal presented with a primary tumor. Compared to the adjacent normal pancreatic tissue, the GFP expression in this tumor was lower (Figure 2G, right), and cancer cells were not completely devoid of nuclear STAT3, suggesting that the retention of active STAT3 might provide a selective advantage of transforming cells *in vivo*.

Selective advantage of cancer cells expressing active STAT3 during PDAC progression

Compared to JAK1-deficient experimental mice, significantly more control animals expressing mutant KRAS in the presence of wild-type JAK1 developed pancreatic tumors. Specifically, five out of 17 control mice not treated with Tam (Figure 3A; *Trp53*^{wt} no Tam)

presented with tumors within 1 year, and eight mice succumbed to PDAC by 16 months of age. Two of these animals had liver and lung metastases at the time of necropsy. The inclusion of one copy of a mutant *Trp53*^{R172H} allele significantly accelerated the tumor onset, and all animals expressing oncogenic KRAS in the presence of mutant p53 and wild-type JAK1 (Figure 3A; *Trp53*^{R172H} no Tam) developed pancreatic cancer after an average latency of 124 days. In comparison to these control groups, we observed a trending extended survival of JAK1-deficient mice expressing KRAS^{G12D} and mutant p53^{R172H} (Figure 3A; *Trp53*^{R172H} + Tam). With a median survival of 151 days, JAK1 conditional knockout mice lived 27 days longer than the controls when Tam was administered early (i.e., after weaning) to delete JAK1 ($p = 0.039$, Gehan-Breslow-Wilcoxon test; log-rank $p > 0.05$). At the histological level, primary pancreatic tumors of untreated control mice were typical adenocarcinoma with variable degrees of desmoplasia (Figure 3B, left). The tumors of Tam-treated mice were similar but exhibited selected areas with distinctive characteristics, such as the presence of columnar cancer cells (Figure 3B, middle). Unlike low-grade preneoplasia in the proximity of the PDACs of Tam-treated mice (Figure 3B, right), the nuclei within the columnar cancer cells were not basally located.

At the time of necropsy, 16 of the 56 untreated controls had macroscopically visible, GFP-negative disseminated tumors in their lungs and livers (Figure 3C). Metastatic lesions were found in 10 of the 14 Tam-treated mice; however, three of these tumors were GFP negative and likely descendants of primary cancer cells that lacked expression of Cre recombinase. Notably, more than 50% of the Tam-treated mice were around 4 weeks older than the untreated controls at the time of necropsy, and the observed GFP-positive metastatic lesions in the livers and lungs of seven Tam-treated mice were small and only identifiable under a fluorescent stereoscope (Figure 3D, left). Two Tam-treated mice also had GFP-positive tumors in their adrenal glands. The immunofluorescent staining results revealed that GFP-positive metastatic cancer cells retained a variable expression of nuclear STAT3 ranging from levels below that of tumor-associated stromal cells to very high levels in cancer cells despite the Cre-mediated activation of the GFP reporter (Figure 3D, right). Tumors with high pSTAT3 expression were likely clonal derivatives where the inducible Cre^{ERT2} led to the activation of GFP but not a complete deletion of both *Jak1* alleles. The absence or incomplete recombination of the *Jak1* conditional knockout alleles was validated by PCR on isolated cancer cells from the two larger GFP-positive adrenal gland tumors (Figure S5). These findings along with the observation that 30% of all metastases were GFP negative suggested that transforming cells that retained active STAT3 had a selective advantage during cancer initiation and progression.

JAK1 is essential for the activation of STAT3, STAT1, and STAT6 in mouse and human pancreatic cancer cells

To address whether JAK1 is required for the persistent activation of STAT proteins as well as the growth and survival of pancreatic cancer cells, we generated six pancreatic tumor cell lines from mice expressing the Flp-activated Kras^{G12D} along with mutant p53^{R172H} in the background of two *Jak1* conditional knockout alleles (Figure S6). Two mice also carried the inactive CAG-LSL-GFP reporter. The presence of the activated *Kras*^{G12D} allele in the tumor cell lines was determined by PCR (Figure S6A). Following a retroviral-based

expression of Cre recombinase, the deficiency in JAK1 was validated in all six cell lines by immunoblot analysis (Figures S6B and S6C). In comparison to the JAK1-expressing parental control cells, the Cre-mediated deletion of this kinase significantly reduced the constitutive activation of STAT3 in steady state (Figure 4A). Deficiency in JAK1 blocked the tyrosine phosphorylation of STAT3 and STAT1 and the formation of STAT3/1 heterodimers in oncostatin M (OSM)-treated cells (Figures S6C−S6E). The deletion of JAK1 also abolished the activation of STAT1 in response to interferon-gamma (INFγ) stimulation (Figure S6F). Like the human PDAC cell lines (Figure 1A), none of the mouse tumor cells expressed active STAT6 in steady state, and deficiency in JAK1 effectively prevented the phosphorylation of STAT6 in response to IL-4 stimulation (Figure 4B). We also generated two pancreatic tumor cell lines from Pdx1-Flp *FSF-Kras*^{G12D} *p53*^{R172H} mice that carry two *Jak2* conditional knockout alleles, and the conditional deletion of JAK2 in these tumor cells did not affect the constitutive activation of STAT3 (Figure 4A). To validate the essential role of JAK1 for the activation of STAT3 in human PDAC cell lines, we used CRISPR-Cas9-mediated gene editing to generate MIA PaCa-2 and AsPC-1 cells that lack JAK1 (Figure 4C). We also established MIA PaCa-2 and AsPC-1 cell lines with a doxycycline (Dox)-inducible knockdown of JAK2. A direct comparison of the parental human cancer cell lines and their JAK1 knockout or JAK2-deficient derivatives demonstrated that, identical to all mouse cell lines, JAK1 is the pivotal Janus kinase that mediates the oncogenic activation of STAT3 (Figure 4C).

While conducting the cytokine response studies, we observed that JAK1-expressing cells retained low levels of active STAT3 following serum starvation and specific growth factor deprivation (Figures S6C, S6D, and S6E), suggesting that, in part, the persistent activation of STAT3 in pancreatic cancer cells is a result of autocrine signaling. Deficiency in JAK1 and the consequential block of the tyrosine phosphorylation of STAT3, STAT1, and STAT6 did not lead to a compensatory activation of STAT5 in steady state and after stimulation with IL-4, IL-13, or OSM (Figure S7A). Interestingly, STAT6 was only activated by IL-4 in PDAC cells but not through stimulation with IL-13 or OSM. While the tyrosine phosphorylation of STAT5 can be induced by human growth hormone (hGH) (Figure S7A, bottom), we found that, unlike in MCF7 human breast cancer cells, STAT5 was not activated in response to hGH stimulation in MIA PaCa-2 cells despite expression of JAK2 (Figure S7C). We also did not observe a compensatory activation of STAT5 when JAK1-deficient mouse and human pancreatic cancer cells and their parental JAK1-expressing controls were transplanted into immunocompromised animals (Figures S7B and S7D).

JAK1 deficiency decreases the proliferation and growth of pancreatic cancer cells *in vivo*

Although JAK1, active STAT3, STAT1, and STAT6 may not be strictly required for cancer cell survival, deficiency in JAK1 had notable effects on the growth characteristics of cancer cells in culture and *in vivo*. Initially, we observed only a marginal decrease in cellular proliferation when mouse JAK1-deficient cancer cells were grown as monolayers (Figure S6G). Interestingly, a pool of JAK1 knockout human AsPC-1 cells could be propagated despite a notable reduction in cell proliferation (Figure S8A), but, unlike MIA PaCa-2 cells, individual AsPC-1 JAK1-deficient clones could not be established (Figures S8B and S8C). Only clones with an incomplete knockout of JAK1 were able to multiply. When grown in

non-adherent culture conditions, mouse and human pancreatic cancer cells with and without JAK1 were able to form similar numbers of tumorspheres (Figure 4D). However, the average size of the tumorspheres was smaller in mouse and human JAK1-deficient cancer cell lines (Figure 4D), which was likely a consequence of the lower proliferative capacity of these cells. In contrast to the reduction in cell proliferation, a knockout of JAK1 did not have any statistically significant impact on cell migration (Figure 4E).

Next, we transplanted mouse and human JAK1 knockout pancreatic cancer cells and their isogenic JAK1 wild-type controls subcutaneously into Athymic nude mice to study the growth characteristics of JAK1-deficient pancreatic tumor cells *in vivo* (Figure 5). In both models, the knockout of JAK1 slowed the growth of tumors (mouse, Figures 5A and 5B; human, 5F, 5G). On the histological level, all tumors were solid adenocarcinomas as shown in Figure 5C. Immunofluorescent staining against the human-specific Ku80 was used to validate the correct xenografting of the parental MIA PaCa-2 cells and their JAK1 knockout derivatives (Figure 5H). In contrast to the high abundance of nuclear STAT3 in the larger control tumors, the knockout of JAK1 was highly effective in sustaining the block of STAT3 activation *in vivo* (mouse, Figure 5D; human, Figure 5I). Explanted cancer cells from the smaller secondary tumors showed that they were composed of JAK1-deficient tumor cells that lack active STAT3 (mouse, Figure 5E; human, Figure 5J). For this study, we purposely used the original pool of MIA PaCa-2 cells with the CRISPR-Cas9-targeted knockout of JAK1 that contained very few cells expressing JAK1 (Figure S8B). However, within the limited experimental timeline, we did not observe a selective amplification of residual JAK1 wild-type cells with active STAT3. The collective results suggest that, while JAK1 and active STAT3 may not be obligatory for pancreatic cancer cell survival, the inhibition of this cancer cell-intrinsic JAK/STAT signaling pathway reduces the proliferation and growth of pancreatic tumor cells *in vivo*.

JAK1 signaling controls the expression of STAT transcriptional targets but does not affect phosphatidylinositol 3 kinase signaling or epithelial and mesenchymal characteristics

In mammary epithelial cells, JAK/STAT pathways are determinants for cell proliferation, survival, and cell death, in part, by modulating the expression of specific Phosphatidylinositol 3 Kinase (PI3K) subunits and AKT that are important downstream targets of receptor tyrosine kinases and RAS GTPase signaling.[22] To assess whether the reduced proliferation of JAK1-deficient pancreatic cancer cells is a consequence of similar signaling networks, we conducted a comprehensive analysis of mitogen-activated protein (MAP) kinase and PI3K signaling in four mouse and three human JAK1-deficient pancreatic cancer cell lines and their parental controls expressing JAK1 (Figure S9). The collective results show that the lack of JAK1 and active STAT3 did not significantly affect the expression and activation of ERK1/2 or AKT in pancreatic cancer cells (Figures S9A and S9B). The p50/p55 regulatory subunits of PI3K are transcriptional targets of STAT3 in the mammary gland epithelium, but it was surprising that both subunits were not expressed in any of the mouse and human pancreatic cancer cell lines (Figures S9C and S9D). In conclusion, pancreatic cancer cells do not seem to have the same molecular networks that facilitate a crosstalk between the JAK/STAT and PI3K/AKT signaling cascades as in mammary epithelial cells.

Next, we examined a potential JAK1/STAT3 dependency of molecular determinants that control cellular plasticity and epithelial identity. The collective results of the immunoblot analyses performed on seven isogenic pairs of PDAC cell lines with and without JAK1 (four mouse and three human) showed that, despite phenotypic variations between parental cell lines, there were no consistent changes in the expression of epithelial and mesenchymal markers (CK19, cadherins, vimentin, and EpCAM) or transcription factors that are known regulators of cellular plasticity such as SNAIL, SLUG, ZEB1, and TWIST (Figures S10A and S10B). The results suggested that active JAK1/STAT3 signaling is not a determinant for the cellular identity of pancreatic cancer cells as previously reported[13] and the observed differences in cancer cell growth properties between JAK1-deficient tumor cells and controls were not a consequence of potential changes in cellular plasticity.

The finding that JAK1/STAT3 signaling does not have a significant impact on cellular plasticity in PDAC is validated by the results of the transcriptomic analysis of six isogenic pairs of mouse pancreatic cancer cell lines with and without JAK1. The multidimensional scaling (MDS) plot shown in Figure S11A illustrates that the gene expression profiles were significantly more divergent between the parental cell lines expressing JAK1 than the differences in gene expression that resulted from the deletion of JAK1. The paired analysis of parental and JAK1-deficient cancer cells identified 245 genes that were downregulated and 65 genes that were upregulated in the JAK1 knockouts (false discovery rate [FDR] <0.05; Figure S11B). Among those, 164 genes were deregulated 2-fold or greater (124 down, 24 up) in cancer cells lacking JAK1. The list of the top 25 deregulated genes (Figure 6A) included *Osmr* and *Il13ra1*, which engage JAK1 for STAT activation (Figures S6C−S6E, and S7A). In agreement with these findings, the gene set enrichment analysis revealed concordant differences in specific gene sets that are functionally related to the interaction of cytokines and their receptors, JAK/STAT signaling, and cell adhesion (Figure 6B). Several of the downregulated genes in the JAK1 knockout cells were STAT3 targets, including *Stat3* itself, *Socs3*, *Map3k8*, and *Tgfbi*, as well as genes encoding selected matrix metalloproteases (MMPs). The deregulated expression of these genes was validated in each cell line using the NanoString nCounter analysis (Figure 6C).

C/EBPδ is upregulated in pancreatic cancer and executes the pro-tumorigenic functions of JAK1 signaling

One of the top JAK1 candidate target genes that were consistently downregulated in JAK1 knockout pancreatic cancer cells was *Cebpd*, which encodes the C/EBPδ (Figure 6A). Contrary to its recently proposed tumor-suppressive role in PDAC,[23] the immunostaining results on human tissue specimens showed that C/EBPδ is considerably upregulated in pancreatic cancers (Figure 7A). While C/EBPδ was not detected in the normal pancreas and low-grade PanINs, high-grade preneoplastic lesions showed a pronounced nuclear expression of C/EBPδ (Figure S12A). Moreover, a significantly elevated expression of this protein was detected in six of nine commonly used human PDAC cell lines (Figures 7B and S12B), including MIA PaCa-2 cells with high levels of active STAT3. The JAK1-dependent expression of C/EBPδ on the level of the protein was validated by immunoblot in mouse and human MIA PaCa-2 cells (Figures 7C, S13A, and S13B, left). Identical to human tissue specimens, C/EBPδ was not expressed in normal pancreata of mice, while cancer cells and

tumor-associated stromal cells exhibited nuclear C/EBPδ at various levels (Figure S14A). The expression of C/EBPδ was significantly lower in JAK1 conditional knockout mice that were treated with Tam after the onset of preneoplasia to delete one or two copies of the *Jak1* gene (Figure S14B). Most notably, C/EBPδ was completely absent in low-grade PanINs in the JAK1 knockout (Figure S14B, right) that lack expression of active STAT3 as shown earlier (Figure 2F, middle). The extended analysis of the expression of other C/EBPs revealed that C/EBPα, C/EBPβ, and C/EBPγ were not present in mouse pancreatic cancer cells (Figure S13A, right), and only the liver-enriched activating and inhibitory protein (LAP, LIP) isoforms of C/EBPβ were detected in human MIA PaCa-2 cells (Figure S13B). The level of the LAP protein was slightly lower in JAK1-deficient cells compared to their parental controls, but the reduced expression of C/EBPβ was less significant than that of C/EBPδ in the JAK1 knockout.

C/EBPδ is encoded by a single exon, which we targeted with high efficiency in MIA PaCa-2 cells using CRISPR-Cas9-mediated gene editing (Figure 7D). The initial results of the knockout experiment confirmed the specificity of the C/EBPδ antibody, and we observed that the high activation of STAT3 remained unchanged, suggesting that C/EBPδ is not an essential mediator of the autocrine loop of inflammatory cytokines that signal through JAK1. Similar to the JAK1 knockout, deficiency in C/EBPδ did not significantly affect the proliferation of cancer cells when they were maintained as monolayers (Figure S15A). However, we observed a significant reduction in the number and average size of tumorspheres when CEBPD knockout cells were grown on non-adherent culture dishes (Figure 7E), suggesting that C/EBPδ may have a role in promoting self-renewal in addition to cellular proliferation. Similar to tumorspheres in culture, C/EBPδ-deficient cells grew significantly slower in xenografted mice compared to the CEBPD wild-type parental controls (Figure 7F).

Next, we generated JAK1 knockout MIA PaCa-2 cells that express exogenous, FLAG-tagged CEBPD to investigate whether the re-expression of C/EBPδ restores the growth of JAK1-deficient tumorspheres. Reinstating the expression of C/EBPδ did not rescue the activation of STAT3 in the absence of JAK1 (Figure 7G) and had no significant effect on the proliferation of cancer cells in monolayer cultures (Figure S15B). However, expression of exogenous C/EBPδ increased the number and average size of JAK1-deficient tumorspheres (Figure 7H). The bright fluorescence of the dTomato reporter, which is co-expressed with CEBPD from the bicistronic lentiviral vector, suggested that the larger tumorspheres were a consequence of the re-expression of C/EBPδ (Figure 7H, right panel). A knockout of C/EBPδ or its re-expression in JAK1-deficient MIA PaCa-2 cells had no effect on the levels of C/EBPβ (Figure S13B, left). More importantly, reinstating the expression of C/EBPδ was sufficient to restore the growth of JAK1-deficient cancer cells in xenografted mice (Figure 7I). The key findings from human MIA PaCa-2 cancer cells were confirmed in mouse pancreatic tumor cells (Figure S16). A genetic rescue of the expression of C/EBPδ in cancer cells with a conditional knockout of JAK1 did not have a major impact on cellular proliferation in monolayer cultures (Figure S16B) but significantly accelerated the formation and expansion of tumorspheres as well as tumor growth in xenografted animals (Figures S16C−S16E). The notion that JAK1 signaling through C/EBPδ is critical for tumor cell proliferation *in vivo* is supported by the analysis of Cyclin D1 expression in transplanted

mouse and human pancreatic cancer cells that are deficient in JAK1 and their parental JAK1-expressing controls (Figure S17). The deletion of JAK1 or C/EBPδ in MIA PaCa-2 cells resulted in a significantly lower nuclear expression of Cylin D1. The reduced level of this pivotal regulator of cell proliferation was rescued by reinstating the expression of C/EBPδ in JAK1 knockout cells. The collective results of this line of investigation suggest that important pro-tumorigenic functions of JAK1 signaling are executed by C/EBPδ.

DISCUSSION

Defining the roles of specific IL-6 class inflammatory cytokines in normal tissue homeostasis and cancer is somewhat complicated because of their functional redundancy, ligand-receptor promiscuity, and the formation of receptor heterodimers within signaling complexes. Then again, the diverse ligand-receptor complexes engage only a few JAKs and STATs for signal transduction, which provides opportunities for targeted intervention, particularly those aimed at blocking the persistent activation of STAT3 in chronic inflammation and cancer. While recent studies highlighted the paracrine contribution of cytokines from the tumor microenvironment,[8,9,24] the oncogenic activation of JAK/STAT signaling in PDAC is likely a primary consequence of autocrine signaling, which is most evident by the constitutive activation of STAT3 in established human and mouse cancer cell lines. This autocrine loop can be effectively blocked through the targeted ablation of JAK1. It should be noted that the downregulation or conditional knockout of JAK2 did not attenuate the activation of STAT3, suggesting that the reported consequences of using various kinase inhibitors in previous studies to target STAT3 activation were incorrectly assigned to JAK2. In addition to STAT3, JAK1 is essential for the activation of STAT1 and STAT6 in pancreatic cancer cells, which is analogous to observations in the normal mammary gland epithelium as well as human and mouse mammary cancer cells.[18–20] These consistent findings among different epithelial tissues and diverse cancer models imply that neither JAK2/3 and TYK2 nor receptor tyrosine kinases (e.g., epidermal growth factor receptor [EGFR]) can substitute for the loss of JAK1 to effectively activate these STAT proteins.

A consequence of the ablation of JAK1 before the onset of PDAC was the predominant presence of low-grade PanINs compared to high-grade preneoplastic lesions in the JAK1 wild-type controls. This suggests that blocking JAK1 signaling arrests the progression of PanIN lesions at an early stage where active STAT3 is typically low or absent. The rare occurrence of palpable tumors in JAK1 conditional knockout mice expressing oncogenic KRAS and the observed delay in cancer progression in animals that also carry mutant p53 support the previously proposed pro-tumorigenic role of STAT3 in pancreatic carcinogenesis.[11,12,25] Our genetic studies show that JAK1 and active STAT3 are not necessary for the survival of pancreatic cancer cells, in particular, when cultured *ex vivo*. However, there was a noticeable growth advantage of cancer cells *in vivo* that escaped from the conditional deletion of JAK1 and that retained expression of active STAT3.

On the mechanistic level, loss of JAK1 resulted in the reduced expression of STAT3 target genes, including MMPs, which are associated with pancreatic and gastrointestinal cancer progression.[12,26,27] Moreover, deficiency in JAK1 blocked the autocrine signaling loop of

inflammatory cytokines by downregulating the receptors for OSM and IL-13 that activate STAT3 and STAT6 in PDAC.[9] Despite differences in the RNA expression of selected genes related to cell adhesion (e.g., *Vcam*, *Alcam*, *Claudins*, and *Syndecans* that are part of this Kyoto Encyclopedia of Genes and Genomes [KEGG] gene cluster), the examination of nine markers of epithelial-mesenchymal transition (EMT) in seven isogenic pancreatic cancer cell lines with and without JAK1 did not provide evidence that JAK1/STAT3 signaling plays a significant role in the modulation of cellular plasticity as previously proposed.[13] It was also surprising to find that, in contrast to mammary epithelial cells,[22,28] STAT3 is not a driver for the transcriptional activation of the PI3K regulatory subunits p50 and p55 or AKT activation, which might explain the limited impact of the JAK1 knockout on pancreatic cancer cell survival.

The identification and validation of *Cebpd* as one of the most consistently downregulated genes in the JAK1 knockout supports earlier studies that C/EBPδ is a target of STAT3.[29,30] The knockout of C/EBPδ in cancer cells mirrored the phenotypic consequences of JAK1 deficiency related to the growth of tumorspheres and reinstating the expression of C/EBPδ was sufficient to restore the tumorsphere-forming properties of human and mouse JAK1-deficient cancer cells and their growth in xenografted mice. However, it should be noted that a high overexpression of *Cebpd* can cause growth inhibition, which might give the impression that this transcription factor is a tumor suppressor.[23] The collective results of this study highlight the oncogenic roles of active STAT3 and C/EBPδ in human and mouse pancreatic cancers. These findings are consistent with earlier reports that implicated C/EBPδ in tumor cell stemness in breast cancer and glioblastoma.[31,32] In summary, JAK1 executes biologically relevant functions of inflammatory cytokines through C/EBPδ in pancreatic cancer cells and may serve as a rational target for PDAC prevention. Although the ablation of JAK1 and STAT3 activation may not lead to pancreatic cancer cell death, the results from the transplantation experiments suggest that targeting JAK1 may slow or prevent the progression of locally invasive disease in patients with resectable pancreatic tumors who are at risk of recurrence.

Limitations of the study

The genetic models in this study provided insight into cell-intrinsic functions of JAK1 signaling and the activation of downstream targets such as C/EBPδ in preneoplastic and fully transformed pancreatic cancer cells. The biological consequences of blocking JAK1 signaling in other cell types within the tumor microenvironment in addition to cancer cells were not investigated but could be therapeutically relevant. Also, the complete absence of the JAK1 protein in cancer cells may not discriminate the potential roles of this kinase as a scaffold independent of its catalytic activity as previously reported for JAK2.[33]

STAR★METHODS

RESOURCE AVAILABILITY

Lead contact—Further information and requests for resources and reagents should be directed to and will be fulfilled by the lead contact, Dr. Kay-Uwe Wagner (kuwagner@wayne.org).

Materials availability—JAK1 and JAK2 conditional knockout mice will be distributed by the Mutant Mouse Resource & Research Centers (MMRRC ID: 71383 and ID: 71382). Mouse tumor-derived cell lines and plasmids created as part of this study are available upon request. A completed Material Transfer Agreement may be required.

Data and code availability

- The RNA sequencing data were deposited in the Gene Expression Omnibus (GEO) under accession number GSE227149.
- This paper does not report original code.
- Any additional information required to reanalyze the data reported in this paper is available from the lead contact upon request.

EXPERIMENTAL MODEL AND STUDY PARTICIPANT DETAILS

Genetically modified mouse strains—Our team generated genetically engineered mice with conditional knockout alleles for JAK1 (*Jak1*^{fl}, *Jak1*^{tm1Kuw})[18] and JAK2 (*Jak2*^{fl}, *Jak2*^{tm1Kuw})[17] as well as the CAG-LSL-tTA transgenic line [Tg(CAG-bGeo,-tTA,-EGFP)2A11Kuw][35] that constitutively expresses the tetracycline-controlled transactivator in a Cre recombinase-dependent manner. The CAG-LSL-GFP reporter strain was kindly provided by Dr. Miyazaki (Osaka University).[36] The TetO-Kras^{G12D} [Tg(tetO-Kras2)12Hev/J][37] and *FSF-Kras*^{G12D} [B6(Cg)-*Kras*^{tm5Tyj}/J][38] mouse strains were purchased from The Jackson Laboratory. Pdx1-Cre[1] transgenics and *Trp53*$^{LSL-R172H}$ knockin mice [B6.129S4-Trp53^{tm2Tyj}/Nci][39] were provided by the NCI Mouse Repository. The conversion of the *Trp53*$^{LSL-R172H}$ targeted locus into the *Trp53*^{R172H} allele was accomplished in the female germline of MMTV-Cre [Tg(MMTV-cre)1Mam] transgenics.[46] A detailed description of the Pdx1-Flp transgenic line and the *Rosa26*$^{CAG-FSF-CreERT2}$ knockin strain expressing a tamoxifen-inducible Cre recombinase in an Flp-dependent manner [MGI:5616874; *Gt(ROSA)26Sor*$^{tm3(CAG-Cre/ERT2)Dsa}$] was published by Schönhuber et al.[40] The transgenes and targeted alleles were maintained on a C57Bl/6 genetic background. PCR primers to genotype transgenes and genetically engineered alleles are provided in Table S1. To induce a Cre^{ERT2}-mediated deletion of the JAK1 conditional knockout alleles and activation of the CAG-LSL-GFP reporter, mice were treated with tamoxifen (Tam) once daily for five consecutive days.[40] All animals were maintained on a 12/12-h light/dark cycle under pathogen-free conditions in micro-isolator cages. The care and use of animals followed the ARRIVE guidelines, and this work was conducted in accordance with the recommendations in the Guide for the Care and Use of Laboratory Animals of the National Institutes of Health. The animal study protocols were approved by the Institutional Animal Care and Use Committees at the University of Nebraska Medical Center and Wayne State University.

Transplant models—To establish xenograft models, suspensions of 1×10^5 pancreatic cancer cells in chilled Matrigel (Corning #354263) were injected subcutaneously into the flanks of 12-week-old male and female NCr$^{nu/nu}$ recipients (Charles River). Tumors were measured using an electronic caliper, and tumor volumes (mm^3) were calculated using the following equation: length (mm) x width^2 (mm^2)/2. The experimental endpoints to assess cancer growth in transplanted recipients and in genetically engineered mice were determined

by the size of the tumor. The maximum allowed tumor size was approximately 1.5 cm in diameter as mandated by the Institutional Animal Care and Use Committees.

Human tissues, multiplexed immunohistochemistry, and quantitative image analysis—Two tissue microarray panels comprising deidentified FFPE normal pancreas tissue and therapy-naïve primary pancreatic cancer from two non-overlapping patient cohorts were provided by the Medical College of Wisconsin Biorepository & Tissue Analytics core as approved by institutional IRB. Histological sections (4 μm) were deparaffinized and went through antigen retrieval using pH 6.0 retrieval buffer (Dako) followed by multiplex immunostaining on a Dako/Agilent Omnis autostainer. Sections were incubated for 30 min with a mixture of rabbit monoclonal anti-pY-Stat3 (Cell Signaling, cat.# 9145; 1:200 dilution) and mouse anti-pan-cytokeratin (AE1/AE3, Dako/Agilent, cat.# M3515, 1:100 dilution), washed and incubated with HRP-conjugated anti-rabbit polymer (EnVision+; Dako/Agilent, cat.# K400311–2, 1:200 dilution), followed by visualization of pY-Stat3 using Cy5-tyramide as substrate. Pan-cytokeratin was visualized using Alexa 555-labeled goat anti-rabbit antibody (Invitrogen, cat.# A-21429; 1:200 dilution). In parallel, separate slides were stained for C/EBPδ (CEBPD) using a pH 9.0 antigen retrieval buffer (Dako) prior to incubation with the rabbit anti-CEBPD antibody (Abcam, cat.# ab245214, 1:1000 dilution) and mouse monoclonal anti-pan-cytokeratin (AE1/AE3, Dako/Agilent, cat.# M3515, 1:400 dilution), followed by HRP-conjugated anti-rabbit secondary antibody. C/EBPδ was visualized using Cy5-tyramide as substrate and cytokeratin was visualized using Alexa 555-labeled goat anti-mouse antibody (Invitrogen, cat.# A-21422, 1:200 dilution). Finally, sections were stained with 4′,6-diamidino-2-phenylindole (DAPI; Vector) to visualize cell nuclei. Stained slides were digitized at 20x magnification on a slide scanner (3DHistech Panoramic Flash II) capturing fluorescent images in three channels (DAPI, Alexa 555, and Cy5). Digitized images were analyzed by Tissue Studio (Definiens), and the mean nuclear expression signal for pY-Stat3 immunoreactivity was computed for cytokeratin-positive cells in each tissue core.

METHOD DETAILS

Genotyping—For PCR-based genotyping of mice, genomic DNA was extracted from digested tail biopsies of mice (10 mg/mL proteinase K in 1% SDS, 50 nM Tris/HCl pH8, 100 nM NaCl, and 50 mM EDTA) using an AutoGenprep2000. The PCR primer sets listed in Table S1 were used to genotype the genetically engineered alleles and transgenes.

To determine the Cre-mediated recombination of the *Jak1* conditional knockout allele in metastases using PCR, pancreatic cancer cells were identified and isolated from H&E-stained histologic sections of GFP-positive tumors in the adrenal glands. Slides were briefly immersed in liquid nitrogen to remove the coverslip and washed in Histo-Clear to remove the mounting media. Metastases were carefully extracted under a stereoscope using a fine needle. The DNA was isolated as described above and the PCRs for the unrecombined floxed and knockout alleles of *Jak1* as well as the wild-type *Jak2* allele (DNA control) were carried out using the primers shown in Table S1.

Histological analysis and immunostaining on mouse specimens—Mouse pancreata and tissue samples from livers, lungs, kidneys, and adrenal glands were placed on glass slides and examined with a Discovery.V8 fluorescent stereoscope (Carl Zeiss, Inc.) for GFP expression. Tissues were fixed overnight in 10% buffered formalin (Fisher Scientific Company) at room temperature and stored in 70% ethanol prior to paraffin embedding, sectioning, and staining with Hematoxylin and Eosin (H&E) for histological examination. Brightfield images were taken on a whole-slide scanner (Leica Microsystems, Inc). For immunostaining, histologic sections of 5 μm were deparaffinized three times in 100% Histo-Clear, rehydrated in decreasing concentrations of ethanol (100%, 95%, 90%, 70%, 50%, and 30% for 3 min each), and washed for 5 min in 1x PBS. Tissue sections were pressure cooked in ImmunoRetriever with Citrate (Bio SB #BSB0022) using a Bio SB TintoRetriever pressure cooker, which was set to 116°C–121°C for 1 min for antigen retrieval. Once the slides had returned to room temperature, they were rinsed for 5 min in 1x PBS and blocked with 3% BSA for 1h. Subsequently, primary antibodies were added (varying dilutions and staining conditions are listed in Table S2) and incubated overnight at 4°C in a moist chamber. The following day, the slides were washed three times with 1x PBS for 5 min each, a fluorophore-conjugated secondary antibody was added, and slides were incubated in the dark for 1h at room temperature in a moist chamber. After washing the slides twice with 1x PBS and once with distilled water, Vectashield DAPI mounting media (Vector, H-1200) and coverslips were applied. Stained slides were examined with an Axio Imager microscope (Carl Zeiss, Inc.) equipped with an SPOT FLEX camera (Diagnostic Instruments, Inc.). For quantification, Cyclin D1-positive nuclei were counted in three representative images (400x magnification) of non-overlapping tumor regions. The relative number of Cyclin D1-positive cells in each of these images was determined with the semi-automated Weka Trainable Segmentation Plugin within Fiji software (v2.0.0; https://fiji.sc/) by counting the Cyclin D1-positive nuclei and the total number of DAPI-stained nuclei. The accuracy of the software was confirmed by manual counting of selected images. Manual counting was performed to quantify Ki67-positive nuclei and the total number of DAPI-stained nuclei within GFP-positive low-grade and high-grade PanINs. Ki67-positive nuclei cells were counted in three representative images (400x magnification) of non-overlapping pancreatic tissue regions. A paired Student's t-test using GraphPad Prism (v6.07; GraphPad Software, La Jolla, CA) was performed to assess statistically significant differences in cellular proliferation. The resulting data were visualized as box and whisker plots with an indication of the minimum and maximum value, as well as the first quartile, median, and third quartile.

Cell culture, CRISPR/Cas9-mediated gene editing, and shRNA-mediated knockdown—Pancreatic cancer cells were derived from primary tumors of mice that express oncogenic KRAS and mutant p53 (Pdx1-Flp *FSF-Kras*^{G12D} *Trp53*^{R172H}) in the presence of two *Jak1* conditional knockout alleles (*Jak1*$^{fl/fl}$). Primary tumor cells were maintained in DMEM medium supplemented with 10% FBS, L-glutamine, and nonessential amino acids as well as 10 μg/mL penicillin/streptomycin and 50 μg/mL gentamicin. To generate isogenic cell lines that are deficient in JAK1, the parental lines were infected with pBabe-Cre-puro retroviral particles and selected with increasing concentrations of puromycin (2, 4, and 7 μg/mL).[43] Immortalized, untransformed human pancreatic cells (HPNE) that were maintained at early and late passage numbers were a kind gift from

Michel Ouellette (UNMC), and the hTERT/E6/E7-immortalized HPNE cells and pancreatic cancer cell line panel were obtained as part of the collaborative work with investigators of the UNMC Specialized Program of Research Excellence (SPORE) in Pancreatic Cancer.[34] Polyclonal MIA PaCa-2 and AsPC-1 cancer cell lines with a CRISPR/Cas9-mediated knockout of JAK1 were generated as a service by Synthego, Corp. MIA PaCa-2 cells were maintained in DMEM medium (ATCC #30–2002) supplemented with 10% FBS and 10 μg/mL penicillin/streptomycin. AsPC-1 cells were maintained in RPMI-1640 medium supplemented with 10% FBS and 10 μg/mL penicillin/streptomycin. The deletion of the *CEBPD* gene in MIA PaCa-2 cells was performed in our laboratory using the Synthego Gene Knockout Kit v2 and Lonza nucleofection protocol (buffer SF). MCF7 cells were obtained from ATCC and maintained in DMEM medium supplemented with 10% FBS, L-glutamine, and 10 μg/mL penicillin/streptomycin.

To conditionally knock down the expression of JAK2 and JAK1 in human pancreatic cancer cell lines (MIA PaCa-1, AsPC-1, and PANC-1), oligonucleotides of previously validated shRNA sequences[47] (Table S3) were cloned into the lentiviral Tet-pLKO-puro vector (Addgene #21915), which permits a doxycycline (Dox)-controlled knockdown of target genes.[41] Lentiviral particles were produced in 293T cells using a standard protocol.[42] Following infection and puromycin selection, pancreatic cancer cells were treated with 2 mg/mL doxycycline for 24 to 72 h to downregulate JAK2 or JAK1. To express exogenous CEBPD in JAK1 knockout MIA PaCa-2 cells and in mouse pancreatic cancer cells with a Cre-mediated knockout of JAK1, we established lentiviral pHIV-*Cebpd*-dTomato and pHIV-*Cebpd*-ZsGreen vectors by inserting an *Xba*I/*Eco*RI fragment of the mouse *Cebpd* coding sequence with a 5′ FLAG epitope tag into the corresponding restriction enzyme sites of the pHIV lentiviral vectors (Addgene #21374, #18121).[42] The correct sequences of the shRNAs and CEBPD expression vectors were validated by Sanger sequencing prior to the production of lentiviral particles. The sequences of the gRNAs and shRNAs that were applied in the gene knockout and knockdown experiments can be found in Table S3.

Cell proliferation, tumorsphere, and cell migration assays—The proliferation rates of pancreatic cell lines were determined by plating 1×10^4 cells into 12 wells of 24-well cell culture plates (CytoOne #CC7682–7524). After 24h, 48h, 72h, and 96h cells were collected from three wells per timepoint and the total number of cells for each well was determined using a CellDrop automated cell counter (DeNovix Inc.). In the case of AsPC1 cells, 2×10^4 cells were plated into each well of a 24-well cell culture plate (Corning #3524). After 24h, 48h, 72h, 96h, 120h, 144h, 168h, and 192h cells were collected from three wells per timepoint and the total number of cells for each well was determined.

For the tumorsphere assays, 1×10^4 cells were plated into 3 wells of 6-well ultra-low attachment plates (Corning #3471) containing regular cell culture media, and tumorspheres were imaged after 7 days using a ZOE Fluorescent Cell Imager (Bio-Rad Laboratories, Inc.). Spheres were counted in at least 8 areas of each plate for quantification. Using the “Colony Blob Count Tool” and appropriate size and shape parameters, ImageJ counted and measured the area of the spheres.

For the *trans*-well migration assays, 0.5 mL of serum-rich media (20% fetal bovine serum, FBS) was added as chemoattractant into a new 24-well plate, and an 8-μm insert was placed in each well (Falcon, 353097). Single cells from the maintenance culture were resuspended in serum-free media and counted using the CellDrop automated cell counter. 1×10^4 cells in 0.3 mL serum-free media were added on top of the 8-μm insert and incubated for 24 h. The following day, the inserts were collected, washed in 1x PBS or distilled water, and consecutively dipped 15 times in HEMA3 fixative. The cytoplasmic and nuclear staining of cells (Wright-Giemsa stain) was carried out using the HEMA 3 STAT Pack (Fisher Scientific, 123–869) according to the manufacture's protocol and washed in distilled water. The membrane inserts were cut out with a razor blade, air dried, and placed in Permount on microscope slides that were then mounted with a coverslip. The number of migrating cells was determined by counting cells under 200x magnification in three areas of 1 mm^2. Data were presented as means of three replicate experiments.

Cytokine stimulation—Cells were maintained in serum-free medium for 16 h and then treated with human growth hormone (500 ng/mL; Invitrogen, Cat.# RP-10928) for 20 min, recombinant mouse IL-4 (50 ng/mL; BD Pharmingen, Cat.# 550067), recombinant mouse IL-13 (50 ng/mL; Peprotech, Cat.# 210–13), recombinant mouse interferon-gamma (10 ng/mL; Millipore, Cat.# IF005) for 15 min or OSM (25 ng/mL; R&D Systems, Cat.# 495-MO) for 15 min, 1 h, 4 h, and 16 h at 37°C prior to cell lysate preparation for immunoblotting.

Immunoblot analyses and immunoprecipitation—Cell pellets or homogenized tissues were sonicated for 3 s in complete lysis buffer containing 1% Nonidet P-40, 0.5% sodium deoxycholate, 0.1% SDS, 1 mM phenylmethylsulfonyl fluoride (PMSF), 0.4 units/mL aprotinin, 1 mM NaF, leupeptin, and 0.1 mM sodium orthovanadate and kept on ice for 30 min. Whole-cell extracts were resolved by SDS-PAGE and blotted onto polyvinylidene fluoride (PVDF) membranes (Invitrogen). The membranes were blocked for 1 h at room temperature in 5% dry milk in 1x TBST (Tris-buffered saline with 0.05% Tween 20) buffer or 5% Bovine Serum Albumin (BSA) in 1x TBST for phosphotyrosine-specific antibodies. Subsequently, membranes were incubated with primary antibodies in the blocking buffer at 4°C overnight. A list of primary and secondary antibodies for immunoblotting as well as recommended dilutions are provided in Table S4. On the next day, membranes were washed three times for 5 min in 1x TBST and incubated for 1h at room temperature with horseradish peroxidase-conjugated secondary antibodies [Digital anti-Mouse-HRP (R1005) or Digital anti-Rabbit-HRP (R1006) from KwikQuant or goat anti-Chicken IgY-HRP (sc-2428) or goat anti-Rat IgG-HRP (sc-2006) from Santa Cruz Biotechnology] in blocking buffer. Membranes were washed three times for 10 min with 1x TBST and then two times for 10 min in 1x TBS (Tris-buffered saline without Tween 20) and finally for 5 min in ultrapure water (Invitrogen 10977–023). Protein bands were detected using the ECL chemiluminescence kit for Western blot analysis [KwikQuant Ultra Digital-ECLTM Substrate Solution (Cat.#R1002)] according to the instructions by the manufacturer (Kindle Biosciences, LCC). Chemiluminescence and brightfield images of the blots with size markers were taken using a D1001 KwikQuant Imager (Kindle Biosciences, LLC). The protein band intensity of the immunoblots was quantified using KwikQuant Image Analyzer

5.9 for Mac OS (Kindle Biosciences, LLC). Membranes were stripped using a mild glycine stripping buffer (Abcam protocol) for consecutive detection of various proteins.

For the co-immunoprecipitation experiment, cells were lysed in complete lysis buffer as described above without the sonication step and incubated with primary antibody and pulled down with DynabeadsTM Protein G according to the manufacturer's protocol (Invitrogen Cat.# 10007D). The immunoprecipitated proteins were analyzed by western blot as described above.

Transcriptomic analyses—Total RNA was isolated from pancreatic cancer cell lines using the RNeasy Mini Kit (QIAGEN). RNA quantity and quality were assessed using a NanoDrop spectrophotometer and gel electrophoresis. The mRNA expression library construction and next-generation sequencing (RNA-Seq) were performed at the UNMC Genomics Core Facility and Novogene. The quality of sequenced reads was evaluated using FastQC (v0.11.9; http://www.bioinformatics.babraham.ac.uk/projects/fastqc). For the differential expression analysis between parental and JAK1 knockout samples, the 150 base paired-end reads were aligned to the GRCm38/mm10 mouse reference genome (UCSC) via Rsubread (v2.0.0).[44] Transcript abundance was determined using the featureCounts function of the Rsburead package, and low abundance gene transcripts (cpm <5 in more than half of the samples) were omitted in further downstream analyses. Subsequently, transcript counts were normalized using the R package edgeR (v.3.28.0).[45] Furthermore, the edgeR package was used for the paired sample differential expression analysis between wild-type parental cells and isogenic JAK1 knockout cells. Genes that passed the threshold of a False Discovery Rate (FDR) below 0.05 were considered significantly deregulated. To visualize the differential expression of select deregulated genes, the genes were log2 transformed and scaled to highlight differences in isogenic cell line pairs and were subsequently plotted as a heatmap using the R-function heatmap.2 (package: gplots v3.0.3), http://cran.r-project.org/web/packages/gplots/index.html. Gene Set Enrichment Analysis (GSEA) was performed using the Broad Institute's GSEA software (GSEA v4.0 for Linux), http://www.gsea-msigdb.org/gsea/downloads.jsp. [48]

The nCounter gene expression analysis was carried out by the Genomics Core of the Research Technology Support Facility at Michigan State University using the NanoString nCounter MAX Analysis System. The resulting data were normalized and visualized using Nanostring's nSolver software (v4.0 for Mac), https://www.nanostring.com/products/analysis-software/nsolver. A list of nCounter design details (genes, sequences) is shown in Table S5.

QUANTIFICATION AND STATISTICAL ANALYSIS

Graphic illustrations and statistics were performed with GraphPad Prism (v6.07; GraphPad Software, La Jolla, CA). All reported measurements were taken from distinct samples. Unless otherwise indicated in the figure legends, experimental data are shown as mean values ± SEM or mean ± SD. For statistical analysis, the data were assessed for normality followed by an unpaired Student's t-test, Mann-Whitney-Wilcoxon test, one-way ANOVA, and Tukey's multiple comparison test. The tumor-free survival distributions between animals

were assessed using the log-rank test or the Gehan-Breslow-Wilcoxon test. p values < 0.05 (*), <0.01 (**), <0.001 (***), or <0.0001 (****) were considered statistically significant.

Supplementary Material

Refer to Web version on PubMed Central for supplementary material.

ACKNOWLEDGMENTS

The authors thank Melissa Anders-DiPonio, Bridget Reno, as well as members of the Animal Model and Therapeutics Evaluation Core and Biobanking and Correlative Sciences Core Facilities at the Karmanos Cancer Institute (KCI) for the preparation of histologic sections. The KCI core facilities are supported by the US Public Health Service grant CA022453. Amalraj Thangasamy assisted with the acquisition of whole-slide images. Immunohistochemistry services were provided by Linna Ge of the Biorepository & Tissue Analytics Core of the Medical College of Wisconsin Cancer Center. RNA sequencing was performed at the UNMC Genomics Core Facility, which is supported by the Public Health Service grant CA036727. The NanoString nCounter data acquisition was carried out at the Genomics Core of the Research Technology Support Facility at Michigan State University. Financial support was provided by Public Health Service Grants CA202917 (K.-U.W.) and CA267549 (H.R.). E.S. is supported by the Intramural Research Program of the National Cancer Institute, in part through contract number HHSN261200800001E. R.D. and M.N.W. were supported by the Ruth L. Kirschstein National Research Service Award T32 (CA009531), and P.D.R. received a graduate fellowship through the Cancer Research Training Program at UNMC (CA009476). N.R. was supported through a research assistantship from the UNMC Graduate Studies Office. The funders had no role in the study design, data collection, analysis, the decision to publish, or the preparation of the manuscript. The illustration for the graphical abstract was generated using BioRender.com.

REFERENCES

1. Hingorani SR, Petricoin EF, Maitra A, Rajapakse V, King C, Jacobetz MA, Ross S, Conrads TP, Veenstra TD, Hitt BA, et al. (2003). Preinvasive and invasive ductal pancreatic cancer and its early detection in the mouse. Cancer Cell 4, 437–450. [PubMed: 14706336]
2. Aguirre AJ, Bardeesy N, Sinha M, Lopez L, Tuveson DA, Horner J, Redston MS, and DePinho RA (2003). Activated Kras and Ink4a/Arf deficiency cooperate to produce metastatic pancreatic ductal adenocarcinoma. Genes Dev. 17, 3112–3126. [PubMed: 14681207]
3. Dennaoui R, Shrestha H, and Wagner KU (2021). Models of pancreatic ductal adenocarcinoma. Cancer Metastasis Rev. 40, 803–818. 10.1007/s10555-021-09989-9. [PubMed: 34491463]
4. Hodge DR, Hurt EM, and Farrar WL (2005). The role of IL-6 and STAT3 in inflammation and cancer. Eur. J. Cancer 41, 2502–2512. 10.1016/j.ejca.2005.08.016. [PubMed: 16199153]
5. Lesina M, Kurkowski MU, Ludes K, Rose-John S, Treiber M, Klöppel G, Yoshimura A, Reindl W, Sipos B, Akira S, et al. (2011). Stat3/Socs3 activation by IL-6 transsignaling promotes progression of pancreatic intraepithelial neoplasia and development of pancreatic cancer. Cancer Cell 19, 456–469. 10.1016/j.ccr.2011.03.009. [PubMed: 21481788]
6. Lesina M, Wörmann SM, Neuhöfer P, Song L, and Algül H (2014). Interleukin-6 in inflammatory and malignant diseases of the pancreas. Semin. Immunol 26, 80–87. 10.1016/j.smim.2014.01.002. [PubMed: 24572992]
7. van Duijneveldt G, Griffin MDW, and Putoczki TL (2020). Emerging roles for the IL-6 family of cytokines in pancreatic cancer. Clin. Sci 134, 2091–2115. 10.1042/cs20191211.
8. Shi Y, Gao W, Lytle NK, Huang P, Yuan X, Dann AM, Ridinger-Saison M, DelGiorno KE, Antal CE, Liang G, et al. (2019). Targeting LIF-mediated paracrine interaction for pancreatic cancer therapy and monitoring. Nature 569, 131–135. 10.1038/s41586-019-1130-6. [PubMed: 30996350]
9. Dey P, Li J, Zhang J, Chaurasiya S, Strom A, Wang H, Liao WT, Cavallaro F, Denz P, Bernard V, et al. (2020). Oncogenic KRAS-Driven Metabolic Reprogramming in Pancreatic Cancer Cells Utilizes Cytokines from the Tumor Microenvironment. Cancer Discov. 10, 608–625. 10.1158/2159-8290.cd-19-0297. [PubMed: 32046984]
10. Scholz A, Heinze S, Detjen KM, Peters M, Welzel M, Hauff P, Schirner M, Wiedenmann B, and Rosewicz S (2003). Activated signal transducer and activator of transcription 3 (STAT3) supports

the malignant phenotype of human pancreatic cancer. Gastroenterology 125, 891–905. [PubMed: 12949733]

11. Corcoran RB, Contino G, Deshpande V, Tzatsos A, Conrad C, Benes CH, Levy DE, Settleman J, Engelman JA, and Bardeesy N (2011). STAT3 plays a critical role in KRAS-induced pancreatic tumorigenesis. Cancer Res. 71, 5020–5029. 10.1158/0008-5472.CAN-11-0908. [PubMed: 21586612]
12. Fukuda A, Wang SC, Morris JP 4th, Folias AE, Liou A, Kim GE, Akira S, Boucher KM, Firpo MA, Mulvihill SJ, and Hebrok M (2011). Stat3 and MMP7 contribute to pancreatic ductal adenocarcinoma initiation and progression. Cancer Cell 19, 441–455. 10.1016/j.ccr.2011.03.002. [PubMed: 21481787]
13. D'Amico S, Shi J, Martin BL, Crawford HC, Petrenko O, and Reich NC (2018). STAT3 is a master regulator of epithelial identity and KRAS-driven tumorigenesis. Genes Dev. 32, 1175–1187. 10.1101/gad.311852.118. [PubMed: 30135074]
14. Arpin CC, Mac S, Jiang Y, Cheng H, Grimard M, Page BDG, Kamocka MM, Haftchenary S, Su H, Ball DP, et al. (2016). Applying Small Molecule Signal Transducer and Activator of Transcription-3 (STAT3) Protein Inhibitors as Pancreatic Cancer Therapeutics. Mol. Cancer Ther 15, 794–805. 10.1158/1535-7163.mct-15-0003. [PubMed: 26873728]
15. Chen H, Zhou W, Bian A, Zhang Q, Miao Y, Yin X, Ye J, Xu S, Ti C, Sun Z, et al. (2023). Selectively targeting STAT3 using a small molecule inhibitor is a potential therapeutic strategy for pancreatic cancer. Clin. Cancer Res 29, 815–830. 10.1158/1078-0432.CCR-22-0997. [PubMed: 36374556]
16. Dong J, Cheng XD, Zhang WD, and Qin JJ (2021). Recent Update on Development of Small-Molecule STAT3 Inhibitors for Cancer Therapy: From Phosphorylation Inhibition to Protein Degradation. J. Med. Chem 64, 8884–8915. 10.1021/acs.jmedchem.1c00629. [PubMed: 34170703]
17. Krempler A, Qi Y, Triplett AA, Zhu J, Rui H, and Wagner KU (2004). Generation of a conditional knockout allele for the Janus kinase 2 (Jak2) gene in mice. Genesis 40, 52–57. [PubMed: 15354294]
18. Sakamoto K, Wehde BL, Rädler PD, Triplett AA, and Wagner KU (2016). Generation of Janus kinase 1 (JAK1) conditional knockout mice. Genesis 54, 582–588. 10.1002/dvg.22982. [PubMed: 27671227]
19. Sakamoto K, Wehde BL, Yoo KH, Kim T, Rajbhandari N, Shin HY, Triplett AA, Rädler PD, Schuler F, Villunger A, et al. (2016). Janus Kinase 1 Is Essential for Inflammatory Cytokine Signaling and Mammary Gland Remodeling. Mol. Cell Biol 36, 1673–1690. 10.1128/mcb.00999-15. [PubMed: 27044867]
20. Wehde BL, Radler PD, Shrestha H, Johnson SJ, Triplett AA, and Wagner KU (2018). Janus Kinase 1 Plays a Critical Role in Mammary Cancer Progression. Cell Rep. 25, 2192–2207.e2195. 10.1016/j.celrep.2018.10.063. [PubMed: 30463015]
21. Rajbhandari N, Lin WC, Wehde BL, Triplett AA, and Wagner KU (2017). Autocrine IGF1 Signaling Mediates Pancreatic Tumor Cell Dormancy in the Absence of Oncogenic Drivers. Cell Rep. 18, 2243–2255. 10.1016/j.celrep.2017.02.013. [PubMed: 28249168]
22. Radler PD, Wehde BL, and Wagner KU (2017). Crosstalk between STAT5 activation and PI3K/AKT functions in normal and transformed mammary epithelial cells. Mol. Cell. Endocrinol 451, 31–39. 10.1016/j.mce.2017.04.025. [PubMed: 28495456]
23. Hartl L, Duitman J, Aberson HL, Chen K, Dijk F, Roelofs JJTH, Dings MPG, Hooijer GKJ, Hernanda PY, Pan Q, et al. (2020). CCAAT/Enhancer-Binding Protein Delta (C/EBPδ): A Previously Unrecognized Tumor Suppressor that Limits the Oncogenic Potential of Pancreatic Ductal Adenocarcinoma Cells. Cancers 12, 2546. 10.3390/cancers12092546. [PubMed: 32906832]
24. Lee BY, Hogg EKJ, Below CR, Kononov A, Blanco-Gomez A, Heider F, Xu J, Hutton C, Zhang X, Scheidt T, et al. (2021). Heterocellular OSM-OSMR signalling reprograms fibroblasts to promote pancreatic cancer growth and metastasis. Nat. Commun 12, 7336. 10.1038/s41467-021-27607-8. [PubMed: 34921158]
25. Chen H, Bian A, Yang L. f., Yin X, Wang J, Ti C, Miao Y, Peng S, Xu S, Liu M, et al. (2021). Targeting STAT3 by a small molecule suppresses pancreatic cancer progression. Oncogene 40, 1440–1457. 10.1038/s41388-020-01626-z. [PubMed: 33420372]

26. Jones LE, Humphreys MJ, Campbell F, Neoptolemos JP, and Boyd MT (2004). Comprehensive analysis of matrix metalloproteinase and tissue inhibitor expression in pancreatic cancer: increased expression of matrix metalloproteinase-7 predicts poor survival. Clin. Cancer Res 10, 2832–2845. 10.1158/1078-0432.ccr-1157-03. [PubMed: 15102692]
27. Tsareva SA, Moriggl R, Corvinus FM, Wiederanders B, Schütz A, Kovacic B, and Friedrich K (2007). Signal transducer and activator of transcription 3 activation promotes invasive growth of colon carcinomas through matrix metalloproteinase induction. Neoplasia 9, 279–291. 10.1593/neo.06820. [PubMed: 17460772]
28. Abell K, Bilancio A, Clarkson RWE, Tiffen PG, Altaparmakov AI, Burdon TG, Asano T, Vanhaesebroeck B, and Watson CJ (2005). Stat3-induced apoptosis requires a molecular switch in PI(3)K subunit composition. Nat. Cell Biol 7, 392–398. [PubMed: 15793565]
29. Zhang Y, Sif S, and DeWille J (2007). The mouse C/EBPδelta gene promoter is regulated by STAT3 and Sp1 transcriptional activators, chromatin remodeling and c-Myc repression. J. Cell. Biochem 102, 1256–1270. 10.1002/jcb.21356. [PubMed: 17471507]
30. Thangaraju M, Rudelius M, Bierie B, Raffeld M, Sharan S, Hennighausen L, Huang AM, and Sterneck E (2005). C/EBPdelta is a crucial regulator of pro-apoptotic gene expression during mammary gland involution. Development 132, 4675–4685. 10.1242/dev.02050. [PubMed: 16192306]
31. Balamurugan K, Mendoza-Villanueva D, Sharan S, Summers GH, Dobrolecki LE, Lewis MT, and Sterneck E (2019). C/EBPδ links IL-6 and HIF-1 signaling to promote breast cancer stem cell-associated phenotypes. Oncogene 38, 3765–3780. 10.1038/s41388-018-0516-5. [PubMed: 30262865]
32. Wang SM, Lin WC, Lin HY, Chen YL, Ko CY, and Wang JM (2021). CCAAT/Enhancer-binding protein delta mediates glioma stem-like cell enrichment and ATP-binding cassette transporter ABCA1 activation for temozolomide resistance in glioblastoma. Cell Death Discov. 7, 8. 10.1038/s41420-020-00399-4. [PubMed: 33436575]
33. Keil E, Finkenstädt D, Wufka C, Trilling M, Liebfried P, Strobl B, Müller M, and Pfeffer K (2014). Important scaffold function of the Janus kinase 2 uncovered by a novel mouse model harboring a Jak2 activation-loop mutation. Blood 123, 520–529. 10.1182/blood-2013-03-492157. [PubMed: 24169825]
34. Lin WC, Rajbhandari N, Liu C, Sakamoto K, Zhang Q, Triplett AA, Batra SK, Opavsky R, Felsher DW, DiMaio DJ, et al. (2013). Dormant cancer cells contribute to residual disease in a model of reversible pancreatic cancer. Cancer Res. 73, 1821–1830. 10.1158/0008-5472.CAN-12-2067. [PubMed: 23467612]
35. Zhang Q, Triplett AA, Harms DW, Lin WC, Creamer BA, Rizzino A, and Wagner KU (2010). Temporally and spatially controlled expression of transgenes in embryonic and adult tissues. Transgenic Res. 19, 499–509. [PubMed: 19821046]
36. Kawamoto S, Niwa H, Tashiro F, Sano S, Kondoh G, Takeda J, Tabayashi K, and Miyazaki J (2000). A novel reporter mouse strain that expresses enhanced green fluorescent protein upon Cre-mediated recombination. FEBS Lett. 470, 263–268. [PubMed: 10745079]
37. Fisher GH, Wellen SL, Klimstra D, Lenczowski JM, Tichelaar JW, Lizak MJ, Whitsett JA, Koretsky A, and Varmus HE (2001). Induction and apoptotic regression of lung adenocarcinomas by regulation of a K-Ras transgene in the presence and absence of tumor suppressor genes. Genes Dev. 15, 3249–3262. [PubMed: 11751631]
38. Young NP, Crowley D, and Jacks T (2011). Uncoupling cancer mutations reveals critical timing of p53 loss in sarcomagenesis. Cancer Res. 71, 4040–4047. 10.1158/0008-5472.CAN-10-4563. [PubMed: 21512139]
39. Olive KP, Tuveson DA, Ruhe ZC, Yin B, Willis NA, Bronson RT, Crowley D, and Jacks T (2004). Mutant p53 gain of function in two mouse models of Li-Fraumeni syndrome. Cell 119, 847–860. 10.1016/j.cell.2004.11.004. [PubMed: 15607980]
40. Schonhuber N, Seidler B, Schuck K, Veltkamp C, Schachtler C, Zukowska M, Eser S, Feyerabend TB, Paul MC, Eser P, et al. (2014). A next-generation dual-recombinase system for time- and host-specific targeting of pancreatic cancer. Nature medicine 20, 1340–1347. 10.1038/nm.3646.

41. Wiederschain D, Wee S, Chen L, Loo A, Yang G, Huang A, Chen Y, Caponigro G, Yao YM, Lengauer C, et al. (2009). Single-vector inducible lentiviral RNAi system for oncology target validation. Cell Cycle 8, 498–504. [PubMed: 19177017]

42. Welm BE, Dijkgraaf GJP, Bledau AS, Welm AL, and Werb Z (2008). Lentiviral transduction of mammary stem cells for analysis of gene function during development and cancer. Cell Stem Cell 2, 90–102. [PubMed: 18371425]

43. Krempler A, Henry MD, Triplett AA, and Wagner KU (2002). Targeted deletion of the Tsg101 gene results in cell cycle arrest at G1/S and p53-independent cell death. J. Biol. Chem 277, 43216–43223. [PubMed: 12205095]

44. Liao Y, Smyth GK, and Shi W (2019). The R package Rsubread is easier, faster, cheaper and better for alignment and quantification of RNA sequencing reads. Nucleic Acids Res. 47, e47. 10.1093/nar/gkz114. [PubMed: 30783653]

45. Robinson MD, McCarthy DJ, and Smyth GK (2010). edgeR: a Bio-conductor package for differential expression analysis of digital gene expression data. Bioinformatics 26, 139–140. 10.1093/bioinformatics/btp616. [PubMed: 19910308]

46. Rädler PD, Vistisen K, Triplett AA, Dennaoui R, Li Y, Shrestha H, Ferraiuolo R-M, Thangasamy A, Saur D, and Wagner K-U (2021). Dual recombinase action in the normal and neoplastic mammary gland epithelium. Sci. Rep 11, 20775. 10.1038/s41598-021-00231-8. [PubMed: 34675248]

47. Neilson LM, Zhu J, Xie J, Malabarba MG, Sakamoto K, Wagner KU, Kirken RA, and Rui H (2007). Coactivation of janus tyrosine kinase (Jak)1 positively modulates prolactin-Jak2 signaling in breast cancer: recruitment of ERK and signal transducer and activator of transcription (Stat)3 and enhancement of Akt and Stat5a/b pathways. Mol. Endocrinol 21, 2218–2232. [PubMed: 17550976]

48. Subramanian A, Tamayo P, Mootha VK, Mukherjee S, Ebert BL, Gillette MA, Paulovich A, Pomeroy SL, Golub TR, Lander ES, and Mesirov JP (2005). Gene set enrichment analysis: a knowledge-based approach for interpreting genome-wide expression profiles. Proc. Natl. Acad. Sci. USA 102, 15545–15550. 10.1073/pnas.0506580102. [PubMed: 16199517]

Highlights

- JAK1 deficiency prevents the formation of high-grade preneoplasia and pancreatic tumors
- Pancreatic cancer cells expressing active STAT3 have a higher propensity to metastasize
- JAK1 is a key signaling node for STAT3, STAT1, and STAT6 activation in cancer cells
- C/EBPδ executes pro-tumorigenic functions of JAK1/STAT signaling

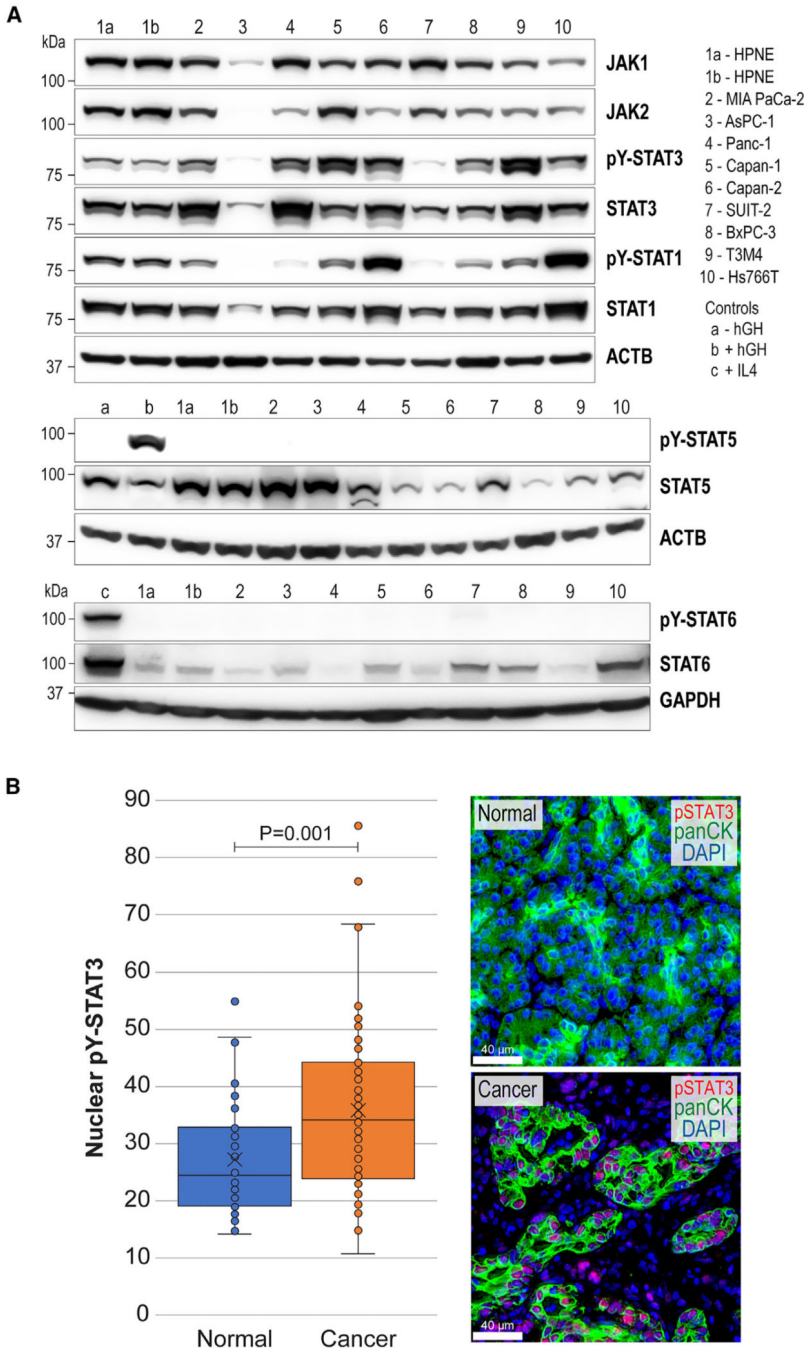

Figure 1. Expression of JAK1 and JAK2 tyrosine kinases and downstream STAT proteins in pancreatic cancer cell lines and tumor tissues

(A) Western blot analyses of JAK1, JAK2, as well as tyrosine phosphorylated STAT proteins in human pancreatic cancer cell lines ($n = 9$) and untransformed pancreatic cells (HPNE). Beta-actin (ACTB) and GAPDH served as loading controls; mouse pancreatic tumor cells treated with human growth hormone (hGH) and IL-4 served as controls for the activation of STAT5 and STAT6, respectively (b and c). Western blots are representative of three experimental replicates used for quantitative analysis in Figure S1A.

(B) Quantitative analysis of nuclear STAT3 expression in primary human pancreatic cancers ($n = 28$) and normal tissues ($n = 17$). The right panel shows representative immunofluorescent (IF) images of normal and tumor tissues co-stained for tyrosine phosphorylated STAT3 (pSTAT3) and pan-cytokeratin (panCK). Slides were counterstained with DAPI; bars, 40 μm.

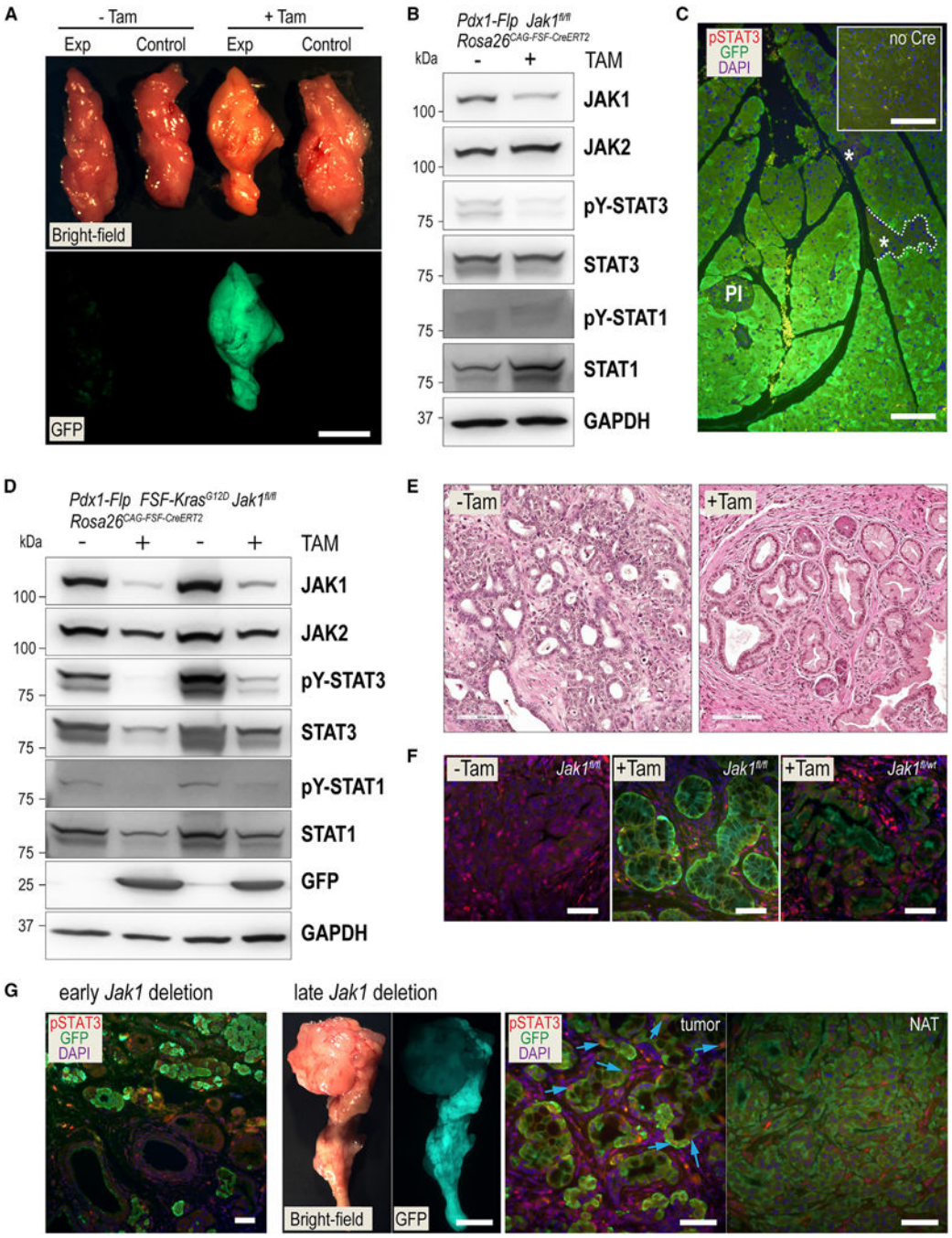

Figure 2. Deletion of JAK1 blocks the formation of KRAS^{G12D}-induced high-grade precursor lesions and pancreatic tumors

(A) Stereoscopic brightfield and GFP fluorescent images of pancreata from adult experimental mice that carry the Pdx1-Flp, *Rosa26*$^{CAG\text{-}FSF\text{-}CreERT}$, and CAG-LSL-GFP transgenes on the background of two *Jak1* conditional knockout alleles (*Jak1*$^{fl/fl}$) before (—TAM) or 2 months after the administration of tamoxifen (+Tam); control, animal without *Rosa26*$^{CAG\text{-}FSF\text{-}CreERT}$; bar, 0.5 cm.

(B) Immunoblot analysis of the expression of JAK1 and JAK2, as well as total and tyrosine phosphorylated STAT3 and STAT1 in pancreata of experimental mice shown in (A). GAPDH served as loading control.

(C) IF staining of GFP and pSTAT3 on a histologic section of a pancreas from a JAK1 conditional knockout. PI, pancreatic islet; asterisks (*) mark areas devoid of GFP. The inset shows the pancreas of a control mouse that lacked the *Rosa26*$^{CAG\text{-}FSF\text{-}CreERT}$; bars, 100 μm.

(D) Immunoblot analysis of JAKs and STATs in pancreata of JAK1 knockout (+Tam) experimental mice expressing mutant KRAS and untreated controls (—Tam).

(E) H&E-stained histologic sections of pancreata from 6-month-old mice expressing mutant KRAS in the presence (left) or absence of JAK1 (right); bars 100 μm. Experimental mice were treated with Tam at 3 weeks of age.

(F) IF staining of pSTAT3 and GFP on KRAS^{G12D}-induced pancreatic precursor lesions of JAK1-deficient mice (+Tam) and age-matched controls expressing JAK1 (—TAM); bars 50 μm.

(G) GFP and pSTAT3 expression in pancreatic tumors of mice that were treated early (3 weeks, left panel) or late in life (6 months, right panel) with Tam to delete JAK1; bars, 50 μm. Brightfield and GFP fluorescent images of the tumor with normal pancreatic tissues adjacent to the tumors (NAT) in a mouse treated with Tam later in life are also shown; bar, 0.5 cm. Blue arrows point to selected GFP-positive tumor cells that retained nuclear expression of STAT3.

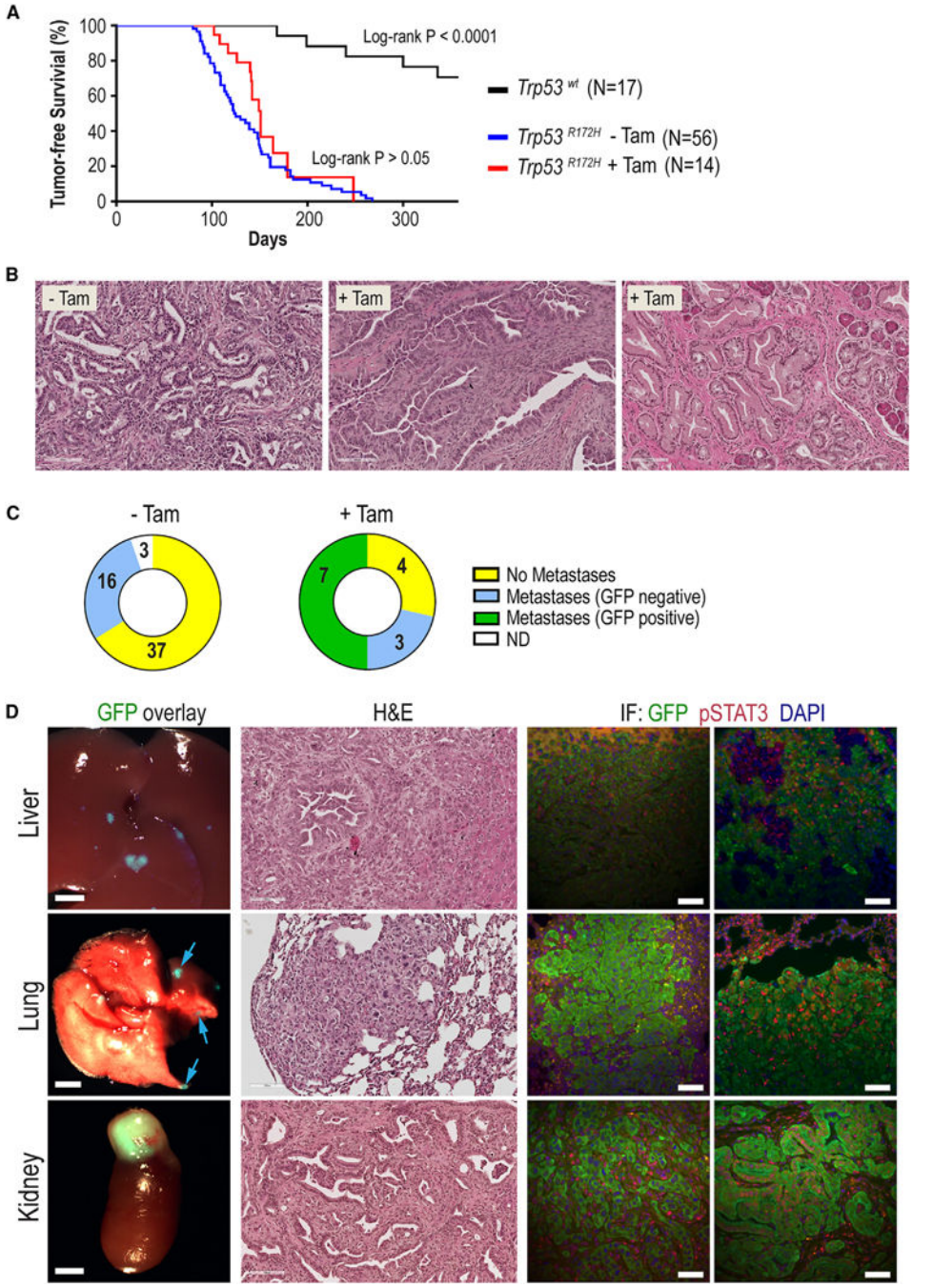

Figure 3. JAK1 and active STAT3 provide a selective advantage during pancreatic cancer progression

(A) Pancreatic tumor-free survival of mice expressing oncogenic $KRAS^{G12D}$ in the background of wild-type p53 (*Trp53*^{wt}) ($n = 17$) or mutant p53 (*Trp53*^{R172H}) that express (—TAM; $n = 56$) or lack JAK1 (+Tam; $n = 14$). Statistical differences between these groups were calculated with the log-rank test.

(B) Histologic sections of pancreatic tumors expressing mutant $p53^{R172H}$ in the presence (—TAM, left) or absence of JAK1 (+Tam, middle). The image on the right shows premalignant lesions in the proximity of a primary cancer of a Tam-treated animal; bars, 100 μm.

(C) Numbers of tumor-bearing JAK1-deficient mice (+Tam) and JAK1-expressing controls (—TAM) that presented no metastatic disease (yellow) or metastatic lesions that were GFP negative (blue) or GFP positive (green) under a fluorescent stereoscope; ND, not determined due to advanced tissue degradation.

(D) Overlay of stereoscopic brightfield images with GFP fluorescence of metastatic lesions (bars, 2 mm) and corresponding H&E-stained histologic sections (bars, 100 μm). Panels on the right show IF images of histological sections with low or high expression of pSTAT3 (red) within GFP-positive metastatic cancer cells. DAPI was used as counterstain; bars, 50 μm.

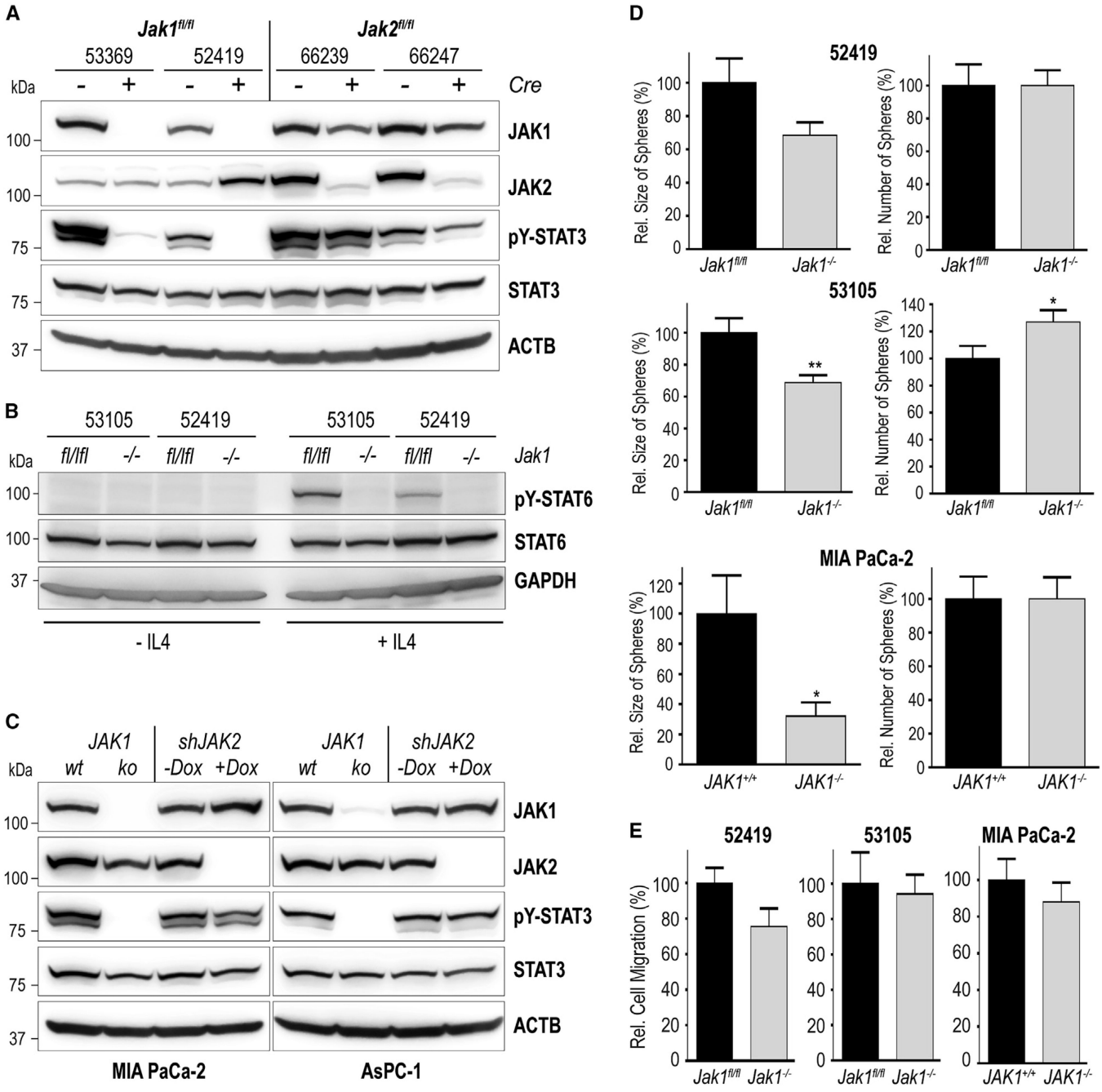

Figure 4. JAK1 is necessary for pancreatic cancer-associated STAT3 activation and pancreatic tumorsphere growth

(A) Immunoblot analysis of STAT3 activation in mutant $KRAS^{G12D}/p53^{R172H}$ mouse pancreatic tumor cell lines before (—Cre) and after the conditional knockout of JAK1 or JAK2 (+Cre).

(B) Western blot analysis of active STAT6 in two JAK1-deficient mouse PDAC cell lines and their JAK1-expressing parental controls with or without IL-4 administration.

(C) Immunoblot analysis of STAT3 activation in two pairs of human PDAC cell lines (MIA PaCa-2, AsPC-1) before and after CRISPR-Cas9-mediated deletion of the *JAK1* gene

and the doxycycline (Dox)-inducible, short hairpin RNA (shRNA)-mediated knockdown of JAK2. ACTB and GAPDH were used as loading controls (A–C).

(D) Comparative analysis of the relative numbers and sizes of tumorspheres in two mouse and one human isogenic cancer cell lines with and without JAK1.

(E) Relative numbers of isogenic mouse and human pancreatic cancer cells that migrated after 24 h in a Transwell assay. Data are presented in panels D andE as the mean ± SD of three replicate experiments. Statistical significance was calculated with t tests; $*p < 0.05$ and $**p < 0.01$. If not indicated otherwise, the differences were not significant.

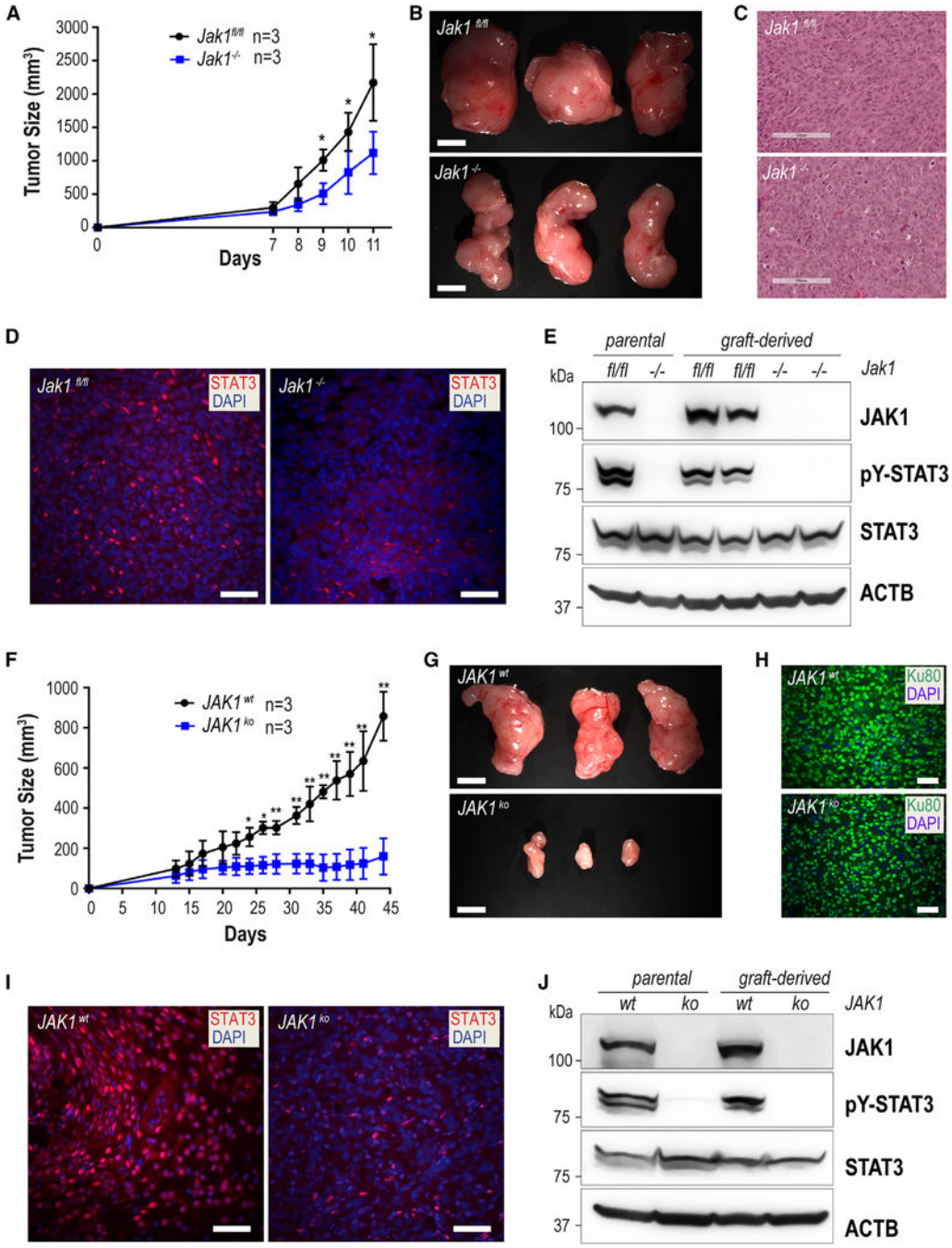

Figure 5. JAK1 deficiency decelerates pancreatic cancer cell growth *in vivo*

(A and F) Growth curves of transplanted mouse (A) and human MIA PaCa-2 (F) pancreatic cancer cells with a Cre recombinase-mediated or CRISPR-Cas9 gene-edited knockout of JAK1 (*Jak1*$^{-/-}$, *JAK1*^{ko}) and their isogenic controls expressing wild-type JAK1 (*Jak1*$^{fl/f}$, *JAK1*^{wt}). The data points shown represent mean values of measured tumor volumes ±SD from three biological repeats per tumor line. Statistical significance between tumor volumes was calculated with t tests; *$p < 0.05$ and **$p < 0.01$.

(B and G) Excised mouse (B) and human (G) tumors at necropsy; bars, 0.5 cm.

(C and H) H&E-stained histologic sections of tumors (C; bars, 100 μm) and IF labeling of the human-specific marker Ku80 (H; bars, 50 μm).
(D and I) IF staining of tyrosine phosphorylated STAT3 in transplanted mouse (D) and xenografted human (I) PDAC cells. Slides were counterstained with DAPI; bars, 50 μm.
(E and J) Immunoblot analyses of JAK1 and active STAT3 on explanted pancreatic cancer cells from the engrafted tumors shown in (B) and (G) in comparison to the parental mouse cell lines (E) or human MIA PaCa-2 cells (J) with and without JAK1. ACTB was used as a loading control.

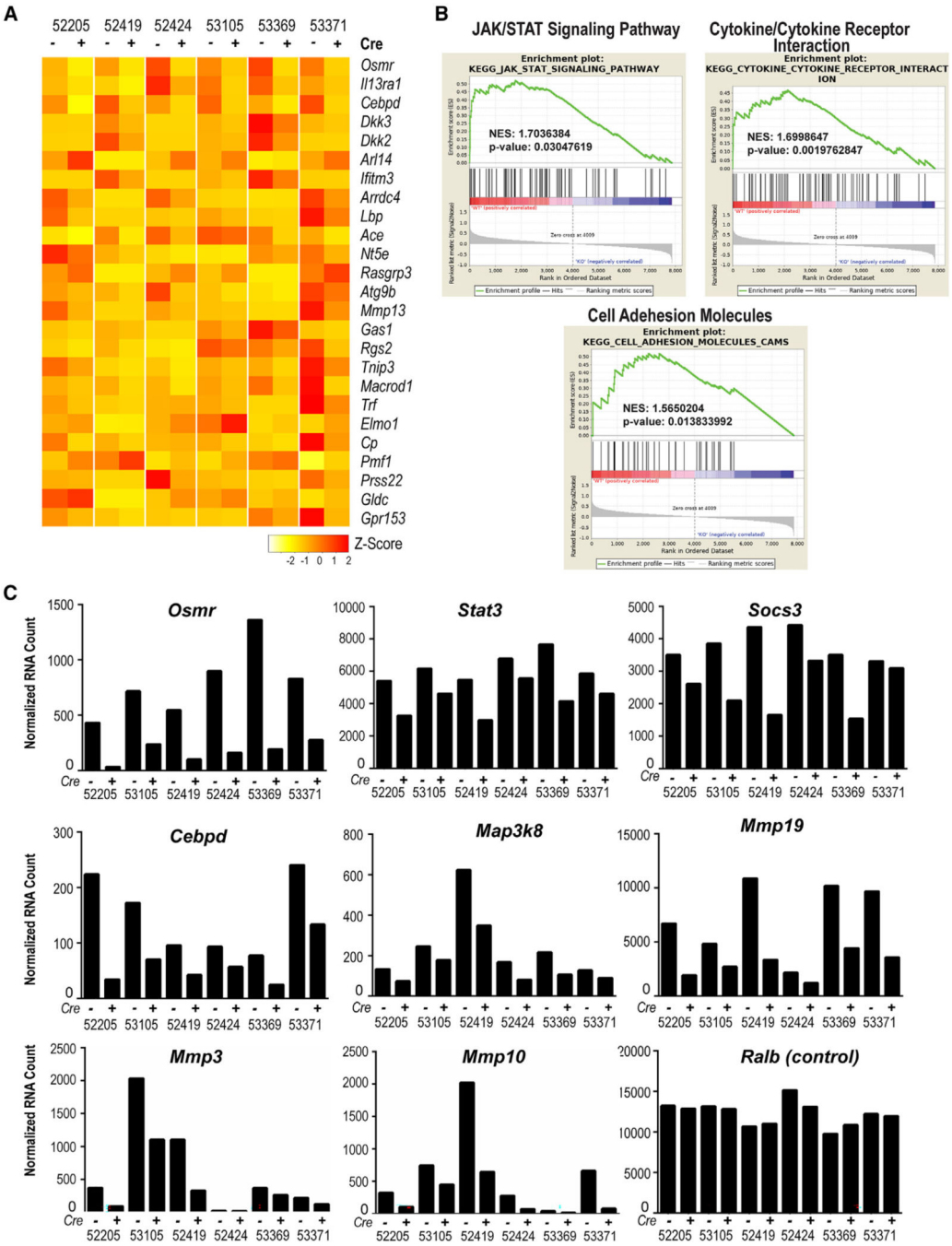

Figure 6. The deletion of JAK1 blocks the transcriptional upregulation of a broad range of STAT target genes

(A) Heatmaps of the top 25 genes that are downregulated (FDR adjusted p values <0.05) in isogenic pancreatic cancer cell lines with a targeted knockout of JAK1 ($n = 6$) compared to their parental controls expressing JAK1 ($n = 6$).

(B) Gene set enrichment plots of selected pathways (enrichment ≥ 1.5 and $p < 0.05$) in JAK1-expressing versus JAK1-deficient cell lines. A positive enrichment score indicates elevated expression of pathway-relevant genes in the JAK1-expressing lines.

(C) nCounter analysis of six isogenic cell lines to validate the downregulated expression of selected STAT target genes in response to the deletion of JAK1 (+Cre). *Ralb*, a ubiquitously expressed gene with low abundance, served as a control.

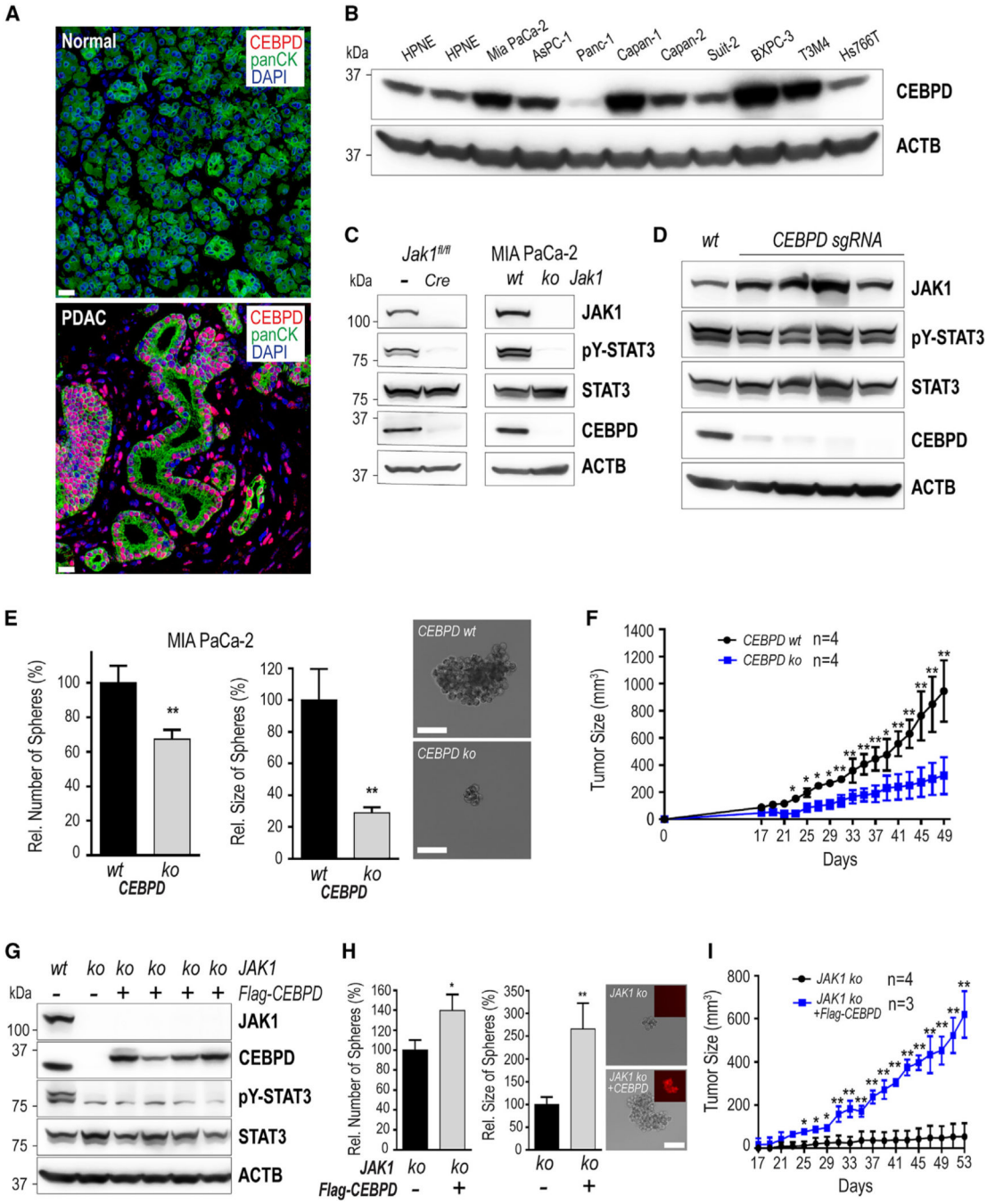

Figure 7. C/EBPδ is a downstream effector of JAK1 signaling that is upregulated in pancreatic cancer cells and that promotes tumorsphere formation

(A) IF staining of C/EBPδ (CEBPD) in the normal human pancreas and pancreatic ductal adenocarcinoma (PDAC); bars, 20 μm.

(B) Immunoblot analysis of CEBPD expression in commonly used pancreatic cancer cell lines ($n = 9$) and untransformed pancreatic cells (HPNE). The immunoblot images are representative of three experimental replicates used for quantitative analysis in Figure S12B.

(C) CEBPD protein expression in isogenic PDAC cell lines before and after Cre-mediated (mouse) or CRISPR-Cas9 gene-edited (MIA PacCa-2) deletion of JAK1 and consequential block of STAT3 activation.

(D) Immunoblot validation of the CRISPR-Cas9-mediated knockout of *CEBPD* in MIA PaCa-2 cells using ribonucleoprotein particles (gRNAs/Cas9 complexes) in four different nucleofection experiments.

(E) Comparative analysis of the relative numbers and sizes of tumorspheres in CEBPD knockout and parental MIA PaCa-2 cells. The right panels show representative brightfield images of tumorspheres; bars, 100 μm.

(F) Growth curves of xenografted MIA PaCa-2 cells that are deficient in C/EBPδ and their wild-type controls; four biological repeats per tumor line.

(G) Expression of FLAG-tagged, exogenous CEBPD in JAK1 knockout (ko) clonal derivatives ($n = 4$, lanes 3–6) of the parental wild-type (lane 1) and JAK1-deficient (lane 2) MIA PacCa-2 cells. ACTB served as a loading control in (B–D) and (G).

(H) Relative numbers and sizes of tumorspheres of multiclonal JAK1 knockout MIA PaCa-2 cells with and without expression of exogenous CEBPD. The right panels show brightfield images of tumorspheres, insets are corresponding fluorescent dTomato images; bars, 100 μm.

(I) Growth curves of xenografted JAK1 knockout MIA PaCa-2 cells with or without exogenous C/EBPδ; $n = 4$ knockout, $n = 3$ knockout with C/EBPδ. The data points shown in (F) and (I) represent mean values of measured tumor volumes ±SD. Statistical significance was calculated with t tests; *$p < 0.05$ and **$p < 0.01$.

KEY RESOURCES TABLE

REAGENT or RESOURCE	SOURCE	IDENTIFIER
Antibodies		
Mouse monoclonal, JAK1	Cell Signaling	Cat#50996; RRID:AB_2716281
Rabbit monoclonal, JAK2	Cell Signaling	Cat#3230; RRID:AB_2128522
Rabbit polyclonal, pY-STAT1	Origene	Cat#TA309955
Rabbit polyclonal, STAT1	Santa Cruz	Cat#sc-592; RRID:AB_632434
Rabbit monoclonal, STAT1	Cell Signaling	Cat#14994; RRID:AB_2737027
Rabbit monoclonal, pY-STAT3	Cell Signaling	Cat#9145S; RRID:AB_2491009
Mouse monoclonal, STAT3	Cell Signaling	Cat#9139S; RRID:AB_331757
Rabbit polyclonal, pY-STAT5	Cell Signaling	Cat#9351S; RRID:AB_2315225
Rabbit polyclonal, STAT5	Santa Cruz	Cat#sc-836; RRID:AB_632445
Rabbit polyclonal, pY-STAT6	Abcam	Cat#ab54461; RRID:AB_882721
Rabbit polyclonal, pY-STAT6	Cell Signaling	Cat#9361; RRID:AB_331595
Rabbit polyclonal, STAT6	Santa Cruz	Cat#sc-981; RRID:AB_632450
Rabbit monoclonal, GAPDH	Cell Signaling	Cat#5174S; RRID:AB_10622025
Chicken polyclonal, GFP	Avēs Labs	Cat#GFP-1020; RRID:AB_10000240
Mouse monoclonal, ACTB	Santa Cruz	Cat#sc-47778; RRID:AB_626632
Rabbit recombinant monoclonal, CEBPD	Abcam	Cat#ab245214; RRID:AB_294368
Mouse monoclonal, CEBPD	Santa Cruz	Cat#sc-135733; RRID:AB_2078197
Mouse monoclonal, CEBPA	Santa Cruz	Cat#sc-166258; RRID:AB_2078042
Rabbit monoclonal, CEBPB	Abcam	Cat#ab32358; RRID:AB_726796
Rabbit polyclonal, CEBPG	Invitrogen	Cat#PA5–121085; RRID:AB_2914657
Rabbit polyclonal, FLAG	Thermo Fisher	Cat#PA1–984B; RRID:AB_558701
Rabbit polyclonal, pERK1/2	Cell Signaling	Cat#9101S; RRID:AB_331646
Mouse monoclonal, ERK1/2	BD Transduction Laboratories	Cat#610123; RRID:AB_397529
Rabbit monoclonal, pT308-AKT	Cell Signaling	Cat#4056; RRID:AB_331163
Rabbit polyclonal, pS473-AKT	Cell Signaling	Cat#9271; RRID:AB_329825
Rabbit polyclonal, AKT	Cell Signaling	Cat#9272; RRID:AB_329827
Rabbit monoclonal, EpCAM	Cell Signaling	Cat#93790S; RRID:AB_2800214

REAGENT or RESOURCE	SOURCE	IDENTIFIER
Rabbit monoclonal, E-cadherin	Cell Signaling	Cat#3195; RRID:AB_2291471
Rabbit recombinant monoclonal, VIMENTIN	Cell Signaling	Cat#5741; RRID:AB_10695459
Rabbit monoclonal, SNAIL	Cell Signaling	Cat#3879T; RRID:AB_2255011
Rabbit monoclonal, SLUG	Cell Signaling	Cat#9585T; RRID:AB_2239535
Rabbit monoclonal, ZEB1	Cell Signaling	Cat#70512T; RRID:AB_2935802
Mouse monoclonal, TWIST	Santa Cruz	Cat#sc-81417; RRID:AB_1130910
Rabbit polyclonal, TWIST	Cell Signaling	Cat#46702S; RRID:AB_2799308
Rabbit monoclonal, p110a	Cell Signaling	Cat#4249; RRID:AB_2165248
Rabbit polyclonal, p85 (p50/p55)	Upstate	Cat#06–195; RRID:AB_310069
Rat monoclonal, CK19	Developmental Studies Hybridoma Bank	Cat#TROMA-III; RRID:AB_2133570
Mouse monoclonal, panCK	Dako/Agilent	Cat# M3515; RRID:AB_2132885
Rabbit monoclonal, Ku80	Cell Signaling	Cat#2180; RRID:AB_2218736
Rabbit monoclonal, Cyclin D1	Abcam	Cat# ab16663; RRID:AB_443423
Rabbit polyclonal, Ki67	Abcam	Cat#ab15580; RRID: AB_443209
Digital anti-Mouse-HRP	Kindle Biosciences	Cat# R1005; RRID:AB_2800463
Digital anti-Rabbit-HRP	Kindle Biosciences	Cat# R1006; RRID:AB_2800464
Goat anti-Chicken IgY-HRP	Santa Cruz	Cat# sc-2428; RRID:AB_650514
Goat anti-Rat IgG-HRP	Santa Cruz	Cat#sc-2006; RRID:AB_1125219
Alexa Fluor 488 goat anti-chicken	Invitrogen	Cat# A11039; RRID:AB_2534096
Alexa Fluor 488 donkey anti-rat	Invitrogen	Cat# A21208; RRID:AB_2535794
Alexa Fluor 594 donkey anti-rabbit	Invitrogen	Cat# A21207; RRID:AB_141637
Alexa Fluor 555 goat anti-rabbit	Invitrogen	Cat# A21429; RRID:AB_2535850
Alexa Fluor 555 goat anti-mouse	Invitrogen	Cat# A21422; RRID:AB_141822
Envision+/HRP-*anti*-rabbit polymer	Dako	Cat# K400311–2
Bacterial and virus strains		
One Shot™ Stbl3™ Chemically Competent E. coli	Thermo Fisher	Cat# C737303
Biological samples		
Mouse: Pancreata	This paper	N/A

REAGENT or RESOURCE	SOURCE	IDENTIFIER
Mouse: Pancreatic tumors	This paper	N/A
Mouse: Lungs	This paper	N/A
Mouse: Livers	This paper	N/A
Mouse: Kidneys	This paper	N/A
Mouse: Adrenal glands	This paper	N/A
Mouse: Mammary glands	This paper	N/A
Human: Normal pancreata	This paper	N/A
Human: Pancreatic tumor tissues	This paper	N/A
Chemicals, peptides, and recombinant proteins		
Tamoxifen	Sigma	Cat#T5648–5G
Puromycin dihydrochloride	Sigma	Cat#P7255–100G
Human growth hormone	Invitrogen	Cat#RP-10928
Doxycycline Hyclate	Sigma	Cat# D9891–25G
Recombinant mouse IL-4	BD Pharmingen	Cat#550067
Recombinant murine IL-13	Peprotech	Cat#210–13
Recombinant mouse interferon gamma	Millipore	Cat#IF005
Recombinant mouse Oncostatin M (OSM)	R&D Systems	Cat#495-MO
Critical commercial assays		
RNeasy Mini Kit	QIAGEN	Cat#74104
HEMA 3 STAT Pack	Fisher-Scientific	Cat#123–869
KwikQuant Western Blot Detection Kit	Kindle BioSciences	Cat#R1002
DynabeadsTM Protein G	Invitrogen	Ref #10007D
Deposited data		
RNA-Sequencing data	This paper	GEO: GSE227149
Experimental models: Cell lines		
Human: HPNE 1a/1b	Gift from M. Ouellette (UNMC) and ATCC	RRID:CVCL_C466

REAGENT or RESOURCE	SOURCE	IDENTIFIER
Human: MIA PaCa-2	ATCC	RRID:CVCL_0428
Human: AsPC-1	ATCC	RRID:CVCL_0152
Human: Panc-1	Lin et al.[34]	RRID:CVCL_0480
Human: Capan-1	Lin et al.[34]	RRID:CVCL_0237
Human: Capan-2	Lin et al.[34]	RRID:CVCL_0026
Human: SUIT-2	Lin et al.[34]	RRID:CVCL_3172
Human: BxPC-3	Lin et al.[34]	RRID:CVCL_0186
Human: T3M4	Lin et al.[34]	RRID:CVCL_4056
Human: Hs766T	Lin et al.[34]	RRID:CVCL_0334
Human: MCF7	ATCC	RRID:CVCL_0031
Mouse: Pancreatic tumor Pdx1-Flp FSF-KrasG12D p53R172H Jak1fl/fl (Cell line 53105)	This paper	N/A
Mouse: Pancreatic tumor Pdx1-Flp FSF-KrasG12D p53R172H Jak1fl/fl (Cell line 52419)	This paper	N/A
Mouse: Pancreatic tumor Pdx1-Flp FSF-KrasG12D p53R172H Jak1fl/fl (Cell line 53369)	This paper	N/A
Mouse: Pancreatic tumor Pdx1-Flp FSF-KrasG12D p53R172H Jak1fl/fl (Cell line 52205)	This paper	N/A
Mouse: Pancreatic tumor Pdx1-Flp FSF-KrasG12D p53R172H Jak1fl/fl (Cell line 53371)	This paper	N/A
Mouse: Pancreatic tumor Pdx1-Flp FSF-KrasG12D p53R172H Jak1fl/fl (Cell line 52424)	This paper	N/A
Mouse: Pancreatic tumor Pdx-FLPo FSF-KrasG12D p53-R172H Jak2 fl/fl (Cell line 66239)	This paper	N/A
Mouse: Pancreatic tumor Pdx-FLPo FSF-KrasG12D p53-R172H Jak2 fl/fl (Cell line 66247)	This paper	N/A
Experimental models: Organisms/strains		
Mouse *Jak1fl, Jak1tm1Kuw*	Sakamoto et al.[18]	MGI:5688302
Mouse: *Jak2fl, Jak2tm1Kuw*	Krempler et al.[17]	MGI:3045140
Mouse: CAG-LSL-tTA Tg [Tg(CAG-bGeo,-tTA,-EGFP)2A11Kuw]	Zhang et al.[35]	MGI:3849835
Mouse: CAG-LSL-GFP	Provided by Dr. Miyazaki (Osaka University)	Kawamoto et al.[36]

REAGENT or RESOURCE	SOURCE	IDENTIFIER
Mouse: TetO-KrasG12D [Tg(tetO-Kras2)12Hev/J]	Purchased from The Jackson Laboratory	Fisher et al.[37]
Mouse: *FSF-KrasG12D* [B6(Cg)-*Krastm5Tyj*/J	Purchased from The Jackson Laboratory	Young et al.[38]
Mouse: Pdx1-Cre	Provided by the NCI Mouse Repository	Hingorani et al.[1]
Mouse: LSL-*Trp53R172H*/+ [B6.129S4-Trp53tm2Tyj/Nci]	Provided by the NCI Mouse Repository	Olive et al.[39]
Mouse: Pdx1-Flp	Schönhuber et al.[40]	MGI:5616872
Mouse: *Rosa26 CAG-FSF-CreERT2*	Schönhuber et al.[40]	MGI:5616874
Mouse: C57Bl/6	Charles River	Strain Code 027
Mouse: NCr$^{nu/nu}$	Charles River	Strain Code 553
Oligonucleotides		
See Table S1 for Genotyping PCR primer sequences	This paper	N/A
See Table S3 for gRNA and shRNA sequence	This paper	N/A
See Table S5 for nCounter elements design	This paper	N/A
Recombinant DNA		
Tet-pLKO-puro	Wiederschain et al.[41]	Addgene, #21915
pHIV-Cebpd-dTomato	This Lab	Designed for this project
pHIV-Cebpd-ZsGreen	This Lab	Designed for this project
pHIV-dTomato	Welm et al.[42]	Addgene, #21374
pHIV-ZsGreen	Welm et al.[42]	Addgene, #18121
pBabe-puro-Cre	This Lab	Krempler et al.[43]
Software and algorithms		
FastQC (v0.11.9)	Babraham Bioinformatics	RRID:SCR_014583
Rsubread (v2.0.0)	Liao et al.[44]	RRID:SCR_016945
edgeR (v.3.28.0)	Robinson et al.[45]	RRID:SCR_012802

REAGENT or RESOURCE	SOURCE	IDENTIFIER
Gplots v3.03	URL: http://cran.r-project.org/web/packages/gplots/index.html	RRID:SCR_025035
GSEA v4.0 for Linux	Broad Institute	RRID:SCR_003199
nSolver software (v4.0 for Mac)	Nanostring	RRID:SCR_003420
Prism v6 (v6.07)	GraphPad Software	RRID:SCR_002798
ImageJ	URL: https://imagej.net/ij/	RRID:SCR_003070
Fiji	URL: https://fiji.sc/	RRID:SCR_002285
KwikQuant Image Analyzer 5.9 for Mac OS	Kindle Biosciences	N/A